ENN Encyclopedia of Nanoscience and Nanotechnology
www.aspbs.com/enn

Diamond Nanostructures Growth

D. C. Barbosa,[1] P. R. P. Barreto,[2] V. W. Ribas,[2]
V. J. Trava-Airoldi,[1] E. J. Corat[1]

[1]*Laboratório Associado de Sensores e Materiais, INPE, Instituto Nacional de Pesquisas Espaciais, CP 515, 12227–010, São José dos Campos, SP, Brazil*
[2]*Laboratório Associado de Plasma, INPE, Instituto Nacional de Pesquisas Espaciais, CP 515, 12227–010, São José dos Campos, SP, Brazil*

CONTENTS

1. INTRODUCTION

The perspectives of nanotechnology developments have a strong focus on carbon-based nanostructures, mainly nanotubes and fullerenes. Nanocrystalline diamond (NCD) and ultrananocrystalline diamond (UNCD) also have a strong potential [1–3] owing to their innumerous superlative properties, comparable to microcrystalline diamond (MCD). For example, the larger hardness among the known materials of the nature; the smaller friction coefficient, which is much desirable for tribological applications [4]; the larger superficial area, which is desirable for electrochemical applications [5]; the larger major adhesion to substrate, ideal for applications in tools industry [6]; the transparency in the visible spectra, which can be used for optical windows; the unusually high thermal conductivity [7]; and the unique capacity to incorporate n-type dopants [8, 9] make them candidate semiconductor for applications in current and future electronics. Besides that, diamond is a noble material, with unsurpassable chemical resistance. It presents corrosion problems only with oxygen at high temperatures (over 800°C), and also presents excellent biological compatibility [10]. With all this potential, diamond, and particularly NCD, became the object of innumerous studies for many applications.

The behavior of diamond crystallite size decreasing down to nanometer scale has been the subject of many pioneering studies. A major advance was achieved with the addition of inert gas in typical MCD deposition conditions. This discovery provided a route to control the microstructure of the diamond film, leading to thick and smooth NCD [11–13].

Even though the inert gas addition is being broadly used and engineered in the development of many applications, the changes in the chemical physical processes occurring during the diamond deposition are not yet well understood. The question of why the NCD grows at this condition actually has been subject of many discussions [14–22]. This chapter has been developed around this important theme. In order to advance in the elucidation of this process, the comparison of the experiments and simulation with and without an inert gas is necessary. This chapter first reviews the growth of diamond microstructures (without the addition of an inert gas) and, second, reviews the influence of inert gas addition in this environment. These reviews are performed by studying two of the most fundamental parameters to uncover the basic chemical process: the dependence on substrate temperature and the dependence on carbon content in the gas mixture. This study reveals that the mechanism for NCD growth is most probably the same of MCD growth, but with a higher competition with the growth of sp^2 carbon phases. At the extreme condition of UNCD growth the competition appears to be so high that the activation process (temperature dependence) favors the sp^2 phases.

1.1. Diamond Growth Environment

At room temperature and atmospheric pressure, graphite is the stable crystalline form of carbon and diamond is thermodynamically stable relative to graphite at high pressures (approximately 150 kbar [23, 24]). The technology to obtain diamond by chemical vapor deposition (CVD diamond) in laboratories became possible owing to a thermodynamically metastable diamond phase, as opposed to the stable graphite phase, founded in the carbon diagram phase. The breaking-through publications to disclose the process were performed by the Japanese scientists in the early 1980s [25]. They were the first to demonstrate that CVD

ISBN: X-XXXXX-XXX-X

diamond growth is possible, provided by certain established conditions that have to be maintained during the growth process.

The necessary condition for CVD diamond growth is the presence of a nonequilibrium gas phase in the region adjacent to the deposition substrate. The nonequilibrium gas phase is generated through gas-phase activation. The gas-phase activation is achieved typically using one of the three basic methods: (1) external heating (as in hot-filament CVD – HFCVD); (2) plasma activation (as in microwave plasma-assisted CVD – MWCVD); and (3) a combination of thermally and chemical activation (as in flame CVD) [26]. Other methods exist but these three have been the subject of the most broaden studies. In the case of NCD deposition the most used methods by scientific community are the microwave plasma CVD and HFCVD.

The microwave plasma CVD is the most used method, in spite of being more expensive than HFCVD. The popularity of this method in scientific community is owing to the high efficiency in dissociation of molecular hydrogen into atomic hydrogen and in the formation of growth precursor species, the two most important characteristics of the activation process for diamond deposition. These characteristics are especially important in the case of NCD deposition, where a lower concentration of molecular hydrogen is used in feed. This method favors a formation of films with high growth rate and quality. Besides, a further advantage of MWCVD is that this system accepts various gaseous mixtures, including mixtures with high oxygen concentration added to argon, hydrogen, and methane frequently used. The fact that no filaments are present in the process makes diamond free of contaminants, ideal for electronic application, for example.

The HFCVD is the most economical and easy to operate of all the methods and produces diamond with very good quality. The main disadvantages are a small film contamination with the filament material and limitation of use of oxygen owing to filament oxidation. However, for applications in which contamination is a minor problem it is the method of choice owing to its low cost and easy scalability. The HFCVD was fundamental to disclose most of the scientific issues concerning the growth mechanism owing to the easier understanding of its only thermal activation process [14, 20–22, 27]. Other processes add more complexity to the study [28, 29]. HFCVD is efficient for the deposition of micro- and nanostructure diamond [25, 30, 31].

The environment for diamond film growth over any type of substrate basically consists in the feeding of a gaseous reagent mixture. For MCD growth this mixture is normally composed of hydrogen and a small concentration of hydrocarbon compounds. For NCD growth a high concentration of an inert gas (in general, argon at more than 50%) is added and for UNCD growth more than 90% of the inert gas is added. This mixture passes through an activation region, where the dissociation of molecular hydrogen into atomic hydrogen occurs. The activation process is the main difference among various diamond growth methods. As explained before, the activation can be obtained thermally, by plasma, by UV radiation or laser, by combustion, or by the combination of these methods. The temperature in the gaseous phase has variations depending on the methods used, but is typically higher than 2000 K. In temperatures of this order the gas is extremely reactive, containing high concentrations of radicals owing to various complex chemical reactions that occur. The activation region is adjacent to the deposition substrate. There are several reviews and books [32–35] that discuss the physical and chemical phenomena that occurs in this region. In summary, the main phenomena are (1) diffusion owing to high temperature gradient present in the process and by atomic hydrogen transport from activation region to the substrate; (2) the forced flow for methods that use high flow rates at the gas inlet; (3) natural convection; (4) diffusion through boundary layer, that is the material diffusion in the interaction surface of gaseous flux with the substrate, mainly for systems at high flow rates; (5) adsorption and desorption on surface owing to chemical process which involved the reactions surface with the gaseous phase; and (6) surface diffusion owing to chemical-physical processes of active species. These stages are fundamentals for diamond films formation, because they are responsible for the transport and incorporation of the gaseous mixture reactants onto the substrate.

Despite the very importance of all the processes involved that establish conditions for the occurrence of such a special process, it is the surface reaction mechanism that enables diamond formation out of all the other possibilities. More aspects of the possible chemical reactions that occur during diamond CVD are discussed below.

1.2. Microstructures of Diamond

Nowadays it is well accepted by scientific community that the MCD growth process is expressed in the following three simple steps [35]:

$$C_DH + H \rightarrow C_D + H_2 \quad (1)$$

$$C_D + H \rightarrow C_DH \quad (2)$$

$$C_DH + C_xH_y \rightarrow C_DC_xH_y \quad (3)$$

where C_D refers to a diamond surface with an open site or dangling bond and C_DH is a hydrogen-terminated surface site. Reaction (I) represents activation of a surface site by of a surface hydrogen atom to produce a surface radical site on the diamond surface (C_D) [35]. Reaction (II) is the recombination of gas-phase atomic hydrogen with the surface radical site, which is very exothermic and is the main responsibility for substrate temperature increase required for hydrocarbon addition (carbon precursors). Reaction (III) represents either a radical (mainly CH_3 [36–38]) or unsaturated molecule (for example C_2H_2) addition to a radical site. This step is responsible for the incorporation of carbon to the surface. Subsequent hydrogen abstraction reactions and CH_3 or unsaturated molecule C_2H_2 additions serve to propagate the growth. Under conditions of CVD diamond growth Reactions (I)-(III) are fast and in steady state [35].

By the end of the 1980s and beginning of the 1990s, there were many suggestions for the main carbon precursor species

that could contribute to diamond formation, CHx or CxHy, each with its own growth rate and propensity to form nondiamond carbon. Thus, not only the quality of the diamond but also the identity of the growth species would depend on the conditions under which the diamond formation took place [39]. Some key experiments where fundamental to shed light into these discussions. It is worth to remember some of them. Martin et al. [39–41] performed a different kind of diamond growth experiment which allowed control of the gas-phase environment above the substrate surface. In their apparatus a hydrogen-argon mixture flowed at a high velocity through a microwave discharge which dissociates some of the molecular H_2 into atomic H. At a point well downstream from the discharge either methane (CH_4) or acetylene (C_2H_2) was added to the flow, and diamond was formed on silicon substrate placed immediately downstream from that point [39]. Since the methane or acetylene did not pass through the discharge, it was expected that the gas-phase chemistry would be drastically simplified and that the species present in the diamond growth region would be closely related to the methyl or acetylene added [39]. The results obtained show that the environment produced by methane injection leads to diamond in greater quantity and higher quality than that produced by acetylene injection. They concluded that acetylene could be a diamond growth species, although a poor one compared to methyl radical (CH_3). In any case they saw that acetylene must be responsible for most of the nondiamond carbon formed, which is to be expected since acetylene is among the most effective growth species for soot and pyrolytic carbon as well as for PAH [39]. Another experiment in the same sense was evaluated by Harris and Weiner [42]. The experiment uses a quartz microprobe and a mass spectrometer to measure how the concentration of acetylene varied with pressure and with the ratio of methane to hydrogen in the input gas. They compared these variations with variations in the mass growth rate. It was found that the apparent reaction order of diamond growth kinetics with respect to methyl radical is the first order but for acetylene it is not first order. But, a simple correlation between methyl radical concentration and growth rate does not prove a cause-and-effect relationship. Nevertheless, if the growth species is indeed either methyl radical or acetylene, then the existence of such a correlation for CH_3 but not for C_2H_2 strongly suggested that CH_3 is the primary diamond growth species in HFCVD [42]. Finally the results obtained by Harris and Weiner suggest that there is little or no cause-and-effect relationship between diamond growth kinetics and the acetylene concentration.

In the meantime, by a numerical simulation model, taking into account only the methyl radical as growth specie, Goodwin and Harris [36, 43–45], supported by theoretical and experimental results, obtained the experimental growth rates, for the most different growth methods, without any adjustable parameter. They proposed a schematic model where the first surface reaction is Reaction (I). Thus, occasionally a gas-phase CH_3 radical can collide and react with the surface reactive site, adding C atom on the surface. Finally, another atomic H comes out of the gas phase and react with the chemisorbed group to create a radical, which interacts with the neighbor C to complete the diamond structure. So, the diamond growth can be considered to be stepwise addition of carbon atoms to the existing diamond lattice, catalyzed by the presence of excess atomic hydrogen [2, 28]. This numerical simulation model was further improved and the other experimental results were obtained by the other authors [37–42], in a way that the scientific community came to a general consensus that the MCD growth should mainly follow a methyl radical mechanism [28].

1.2.1. The Important Role of Atomic Hydrogen

From the diamond growth reaction mechanisms it is possible to note that despite methyl radical, the atomic hydrogen also plays an important role in the CVD diamond growth, which leads it to be considerate as a critical component driving the deposition chemistry. Is general knowledge that a high concentration of atomic hydrogen drives to the obtaining of a diamond with good quality and preferential MCD deposition. The deposition process is extremely complex [22, 28, 35, 36, 46, 47] and is not really completely described by the proposed mechanisms mainly owing to a competition for deposition between carbon with hybridization sp^3 (diamond) and sp^2 (graphite) and the various chemical reactions that can occur. In this aspect, the atomic hydrogen plays an essential role, suppressing the nucleation and the growth of the graphitic structures [48–50]. This occurs owing to the fact that atomic hydrogen etches the graphite 3–4 orders of magnitude faster than diamond [51], then the graphite and the other phases that are not diamond are removed from the substrate.

The important aspects of atomic hydrogen in the MCD growth are (1) the gas-phase conversion of hydrocarbons in radicals, or precursors, essential for the diamond formation [52, 53]; (2) preferential etching of sp^2 carbon during deposition allowing the evolution of high-quality diamond films [53]; (3) the hydrogen abstraction, which induces a sites creation where the precursors are adsorbed [54], allowing the sequence of diamond growth; and (4) the diamond cluster and substrate surface stabilization, which maintains the sp^3 hybridization configuration, allowing nucleation and growth, and removing the thermodynamic barrier which causes graphitic rather than diamond growth [28, 53].

The concentration of atomic hydrogen present in the system also can modify the properties of diamond films [54, 55], for example, (1) hydrogen is necessary to induce surface conductivity on diamond, owing to a low electron affinity of hydrogenated diamond surface [56]; (2) hydrogen can induce negative electron affinity on diamond surfaces by chemisorption [54, 57], the formation of C–H dipoles is considered to be the origin of the negative electron affinity of hydrogen-terminated diamond [58]; and (3) hydrogen allows to control doping in conjugation with boron atoms [54, 59], the understanding of hydrogen incorporation is crucial for a proper control of the conductivity of boron-doped diamond films [59].

Finally, the atomic hydrogen is the most critical component in the CVD gas-phase mixture and indeed drives the whole chemical process. Nevertheless, in the recent years, some works investigated the effect of changing the hydrogen content by, for example, the addition of inert gases [11–13]. These works are relevant to the achievement of

understanding of the factors that control the crystal size obtained by CVD of diamond and to reach the insights necessary for the synthesis of NCD films.

1.3. Nanostructures of Diamond

The study of nanostructure diamond synthesis begins in the first years of the 21st century. Actually many investigations have been carried out in order to study the effect of nucleation on the growth of NCD films [14–22], specially because the controlled inert gas addition in the growth environment, besides promoting the control of diamond grain size, also appeared to modify the CVD diamond kinetic process.

For example, especially in the HFCVD method, the use of high percentage of argon alters the convection of molecular hydrogen that arrives in the hot-filament and the consequence of its diffusion. This process commits the function of a hot filament, which produces a sufficient quantity of atomic hydrogen to decompose the methane to form possible precursors. This decrease in molecular hydrogen diffusion is observed experimentally, since further independent heating is necessary for the substrate temperature to be ideal for growth. This reduction in the temperature of the substrate, as a function of feeding inert gas, is caused by the weakness of recombination reaction of atomic hydrogen with the growth surface, and, to a less extent, is also caused by the differences in the thermal conductivity of inert gas and hydrogen. Owing to a little molecular mass, the thermal conductivity of hydrogen is 10.5 times larger, for example, than argon. These facts change the fluid dynamics promoting a depreciation of heat transfer from the activation region to the substrate.

The chemical reaction that occurs during NCD deposition is present subject of many discussions of scientific community. While the MCD growth model is relatively well accepted, the NCD growth models are very controversial. In this sense, some models propose that, in the case of nanostructures of diamond, C_2 dimers play a dominant role in the renucleation process to form nanostructures [3, 15, 17, 60], opposing microstructured diamond, where C_1 species are the main growth species considered. More recent experimental works [16, 61, 62] have reported that C_2 does not play a major role in the formation of nanostructures of diamond, and other works [14, 16, 47] report a unique model for the different diamond structures.

The most important work to try explaining the chemical reactions that occur during diamond nanostructures growth in recent days is proposed by Paul May and Mankelevich [14, 47, 63]. This work has been of good acceptance by the scientific community because it consists of a unique model for any dimensional structure of diamond. They suggest that in the growth of diamond nanostructures, many species are present in the activation region, including H^+, CH_3, C_2H_2, CH_2, CH, C, as well as C_2, and several of these species could take place in the growth process, but the CH_3-driven mechanism continues to be the predominant one for conditions where H_2 concentration is high. Given the concentrations of species near the diamond growth surface, this model presents two mechanisms which affect the normal diamond structure propagation: the appearance of a surface carbon atom with two dangling bonds C_2Hy, followed by the adsorption of other gas-phase hydrocarbon radicals. This causes the restructuring of the surface and the growth of the next layer before filling all the voids of the current layer, which can occur at high CH_3 addition rate, or more exactly, at elevated gaseous $\Sigma CHx/H$ ratios, $x < 4$ [64]. Finally, the NCD chemical growth steps are the same as MCD, but in the NCD growth case Reaction (III) is in a state where not only methyl radical (CH_3) is the precursor carbon of diamond surface growth but also the other radicals become nonnegligible compared to CH_3 and hydrogen concentration [14].

1.3.1. The Important Role of Argon

The utilization of an inert gas, especially argon, in high concentrations in the diamond CVD, mixed to hydrogen and methane frequently used, represents an innovation for the 21st century. The growth environment is considerably modified with the insertion of this new gas. The argon feeding percentage provides a control of grain size of diamond obtained by CVD method. This is easy to see in Figure 1 that shows the SEM micrographs of CVD diamond obtained at different argon concentrations in the feed gas. MCD growth is observed without argon addition. A drastic morphological change is possible to observe with 75 vol.% of

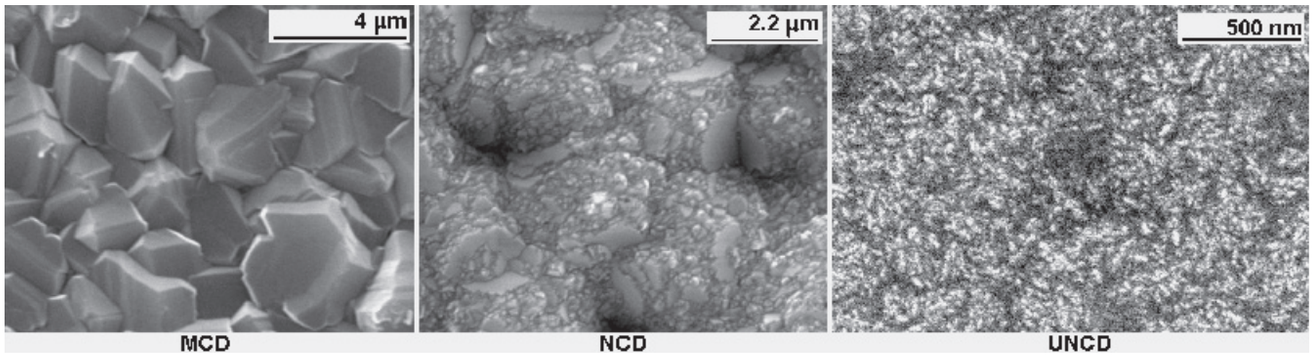

Figure 1. SEM images of diamond films morphology obtained in a HFCVD reactor using a gas mixture of: (MCD) 1 vol.% CH_4 in H_2; (NCD) 75 vol.% Ar, 0.5% CH_4, and 24.5 vol.% H_2; and (UNCD) 90 vol.% Ar, 1 vol.% CH_4, and 9 vol.% H_2. The samples were grown at 800°C substrate temperature.

argon. From this argon concentration the diamond crystals begin to lose the micrometric character and start to present a new structure, composed by nanometric diamond grains sizes (less than 100 nm). Likewise with 90 vol.% of argon, the grains present ultrananometric diamond morphology (size less than 10 nm). Therefore, increasing the argon gas content in the growth environment promotes the decrease of diamond grain size and also influences the morphology of the grown sample.

Another change observed by the insertion of argon in the CVD of diamond is the change of quality of deposited film, as observed by Raman spectroscopy at 514.5 nm laser excitation, Figure 2. The quantity of sp^2-bonded carbon signatures, evidenced by the broad features detected around 1550 cm^{-1}, increases proportionally with the argon content, and a new band appears around 1150 cm^{-1}. The 1150 cm^{-1} band is correlated with the presence of transpolyacetylene at the grain boundaries and surfaces [65], and is typically found in diamond nanostructures. So, this behavior of increasing of sp^2 compounds with the argon concentration and the appearance of new band in 1150 cm^{-1}, correlated to NCD structures, is so expressive that causes a masking of the 1332 cm^{-1} peak, corresponding to diamond structure. The 1332 cm^{-1} Raman peak may only be revealed with laser excitation in the UV, where the Raman sensitivity to sp^2 carbon is considerably decreased [66, 67].

These new bands that appear in the Raman spectrum mainly indicate the existence of a larger number of sp^2 defects in the films structure. These defects can be attributed to a high renucleation process. This high defect density

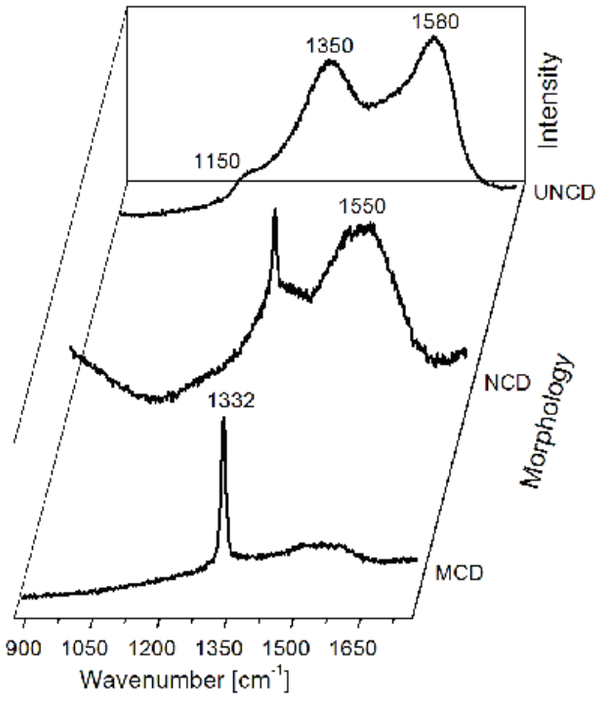

Figure 2. Raman spectra of corresponding films of Figure 1. The spectrum was obtained by micro-Raman-scattering spectroscopy with excitation at 514.5 nm (Renishaw microscope system 2000).

observed by Raman spectra is coherent with the morphology of grains observed in the films deposited with high argon concentration. This is confirmed by the morphology of NCD and UNCD films, where it is observed that the film texture is formed by coalescence of ball-like structures.

To explicitly elucidate the function of argon addition it is necessary to compare experiments with argon (NCD and UNCD growth conditions) and without argon (MCD growth conditions). Many authors performed such kind of investigations [11–13, 68] and the results obtained indicate that high methane concentration as well as argon addition both has effect on the formation of diamond nanostructures. These studies are subject of intense discussions [14–22]. In order to elucidate the underlying mechanism of argon in the CVD diamond systems, in the next sections we will discuss further the influence of substrate temperature and methane concentration for MCD, NCD, and UNCD growth.

2. INFLUENCE OF SUBSTRATE TEMPERATURE

The determination of temperature dependence with diamond growth parameters can give critical information regarding the rate-limiting steps during deposition. The substrate, the growth rate dependence with temperature, for example, is an essential parameter when discussing growth kinetics. The activation energy, determined from the Arrhenius plot, shown in eqn (1), of the diamond growth rate dependence as a function of the substrate temperature, can provide significant insight into the chemical kinetics on the growth surface

$$G \propto \exp\left(\frac{-E_a}{RT_S}\right) \tag{1}$$

where G is the measured growth rate, E_a the activation energy to be found, R the gas constant, and T_S the measured substrate temperature.

Even though the activation energy measurement can disclose a growth mechanism if the value obtained corresponds to the limiting step of some reaction mechanism, a lot of misleading information may be obtained without a deeper evaluation: (1) the growth dependence on substrate temperature may depend not only on the reaction mechanism but also on the reagent concentrations involved, which may complicate significantly the interpretation even for a simple mechanism; (2) competing growth mechanisms may contribute to a merged and inseparable temperature dependence; (3) other important issue is the method to measure growth rate which should be completely independent of growth temperature. For example, thickness growth measurement is probably valid to a limited extent since conditions of high void and defect formation may significantly change film specific mass; and (4) some experimental errors, but to less extent, may also impact the measured values of activation energy, as errors in substrate temperature measurement, or errors in the growth time measurement owing to the low accuracy of determining

the induction period (time period to onset nucleation), which may be strongly temperature dependent.

For MCD growths there are several measurements of activation energy and there is a review [20, 69] that shed some light on the interpretation of most of these experiments. For NCD growth the number of papers on this topic is rather limited [17–19, 70]. For this, it has still not been clarified whether gas phase or surface effects are responsible for the NCD formation. The comparison of the influence of MCD, NCD, and UNCD deposition with the substrate temperature is an important investigation in order to get insight into this view.

2.1. Microstructures of Diamond

Many studies have reported measurements of the dependence of MCD growth with substrate temperature, either for growth of polycrystalline or single-crystal diamond**,** using different diamond CVD method and gas mixtures [71–80]. Most of these studies found an Arrhenius behavior and determined activation energy. Some of the earlier determinations of the activation energy have shown a value in the range of 20–30 kcal mol^{-1} [71–73]. However, many other studies have shown much lower activation energies [70, 74–80]. Corat et al. [20, 69] evaluated most different values found in the literature, by plotting all of them together, through a normalized growth rate as a function of substrate temperature. From this plot a unique tendency for the MCD activation energy around 10 kcal mol^{-1} was found. This evaluated comparison suggests that at least in the range from around 600 to 900°C, there is a common process for MCD, independent of the CVD diamond growth method and the gas system. Among all the experimental results reviewed there were HFCVD, MWCVD, arcjet plasma CVD, and flame growth, using different gas mixtures containing only hydrogen and methane, but also with the addition of oxygen and halogens.

To help understand this higher end of temperature dependence, there is an important simulation paper by Warnatz and coworkers [81–83]. With a surface reaction mechanism based on CH_3 growth, considering 15 surface reactions and gas-phase concentrations calculated by an one-dimensional mechanism, they fitted the growth dependence on temperature obtained experimentally by Chu et al. [84]. They correctly fitted the value around 20 kcal mol^{-1}. This value showed that their eqn (15) was the limiting step but with the contribution of atomic H and CH_3 concentrations on gas phase nearby the surface. H and CH_3 concentrations contributed to the reaction kinetics.

This value, around 20 kcal mol^{-1}, is one of the earliest measurements of activation energy, and Corat et al. [20, 69] attributed it to a low content of atomic hydrogen in the gas phase as possible in earliest HFCVD systems. The value, around 10 kcal mol^{-1}, is obtained in reactors with much higher H content. Warnatz and coworkers [81–83] show that the temperature dependence of the rate coefficient of their reaction (15) can be characterized by a net activation energy of around 10 kcal mol^{-1}. "Reaction 15, the bridging of an adsorbed CH_3 molecule, is identified as the rate-limiting step to form diamond" [81]. A simple evaluation of Warnatz model shows that their reaction (15) is the limiting step of the process and the activation energy around 10 kcal mol^{-1} is obtained if H concentration is sufficiently high for the reaction kinetics to be independent of H and CH_3 concentrations.

Other intricate observation shown by MCD growth measurement of activation energy is its steep reduction at lower temperatures. Some authors suggested that probably other mechanisms should contribute to lower temperatures. However, another observation shown by Corat et al. [20, 69] was that the steep reduction of activation energy was not observed if mass growth rate was measured instead of thickness growth rate, at least down to 420°C. If mass growth rate is considered, around 11 kcal activation energy of reaction (15) of Warnatz [81–83] papers is valid down to 420°C. This leads to the conclusion that the growth mechanism, based on CH_3 incorporation, is the same in this whole temperature range and that only film specific mass varies at lower temperatures.

Items (1) and (3) shown in the foreword of this section are clearly addressed in the above discussion. Probably item (4) is the reason for most variation of closer values among different authors. But the observation of the whole set of data observed in the literature and plotted together by Corat et al. [20, 69] shows clearly that a unique mechanism exists. Even newer experiments, with different gas mixture [79], fit quite well to the whole set of experiments. Only with this more complete analysis and with the help of Warnatz model [81–83] it is possible to suggest, from the activation energy measurements, that for MCD growth there is a strong evidence of a unique CVD diamond growth mechanism, which is based on methyl radical incorporation.

Any further assumption of a possible new growth mechanism should carefully address all the items cited. For this reason we prepared careful experiments to measure the activation energy for NCD and UNCD growth in HFCVD. Basically, a reactor was constructed with an independent control of substrate temperature. The substrate holder was designed to have uniform temperature. Multiple straight filaments were used to guarantee the production of enough atomic hydrogen to operate in a regimen in which reaction (15) of Warnatz model [81, 83] proceeds independent of H and CH_3 concentrations. Previously grown diamond substrates were used to minimize the induction period. The most important detail, mass growth rate, was used to evaluate the activation energy.

The first test of this system and method was the measurement of activation energy in MCD conditions. The schematic of the reactor with multiple straight filaments is shown in Figure 3. The experimental apparatus has independent substrate temperature control over substrate temperatures between 600 and 800°C, provided by an extra heating under the substrate holder. The sketch of the substrate holder is shown in Figure 4. Basically it is composed of a ceramic body with a tungsten filament inside to heat the flat niobium substrate holder. Substrate temperature is measured by a chromel-alumel thermocouple in contact with the niobium substrate holder. Substrate temperature was the only parameter changed in all the experiments. The feed gas mixture was 1 vol.% methane balanced with hydrogen. The filaments were kept at 2200°C and checked using an

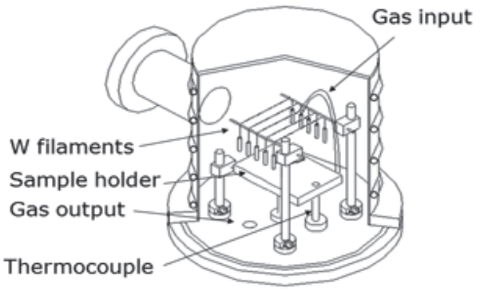

Figure 3. Experimental setup. Detail of the HFCVD reactor used.

uncorrected disappearing filament pyrometer. The distance between the filament and the substrate was 5 mm, and the typical deposition time was 5 h.

For a more accurate study of the diamond film properties and their activation energy, two samples sets were put together in each deposition experiment. The first concerns the diamond films grown on diamond substrates. The second set concerns the diamond films grown on silicon substrates. It is important to point out that the samples were grown together to keep similar experimental conditions, as may be observed in Figure 4.

The characterizations by scanning electron microscopy (SEM) were performed on the films obtained on silicon substrates. The silicon substrate was single-crystal p-type (1 0 0) of resistivity 1–20 Ω cm. Silicon was pretreated in an ultrasonic bath with a 250 nm diamond powder suspension in hexane for 1 h and then cleant in acetone for 5 min. The samples grown on the diamond substrate were used to compute the mass growth rate. The diamond substrates were previously grown on graphite substrate in a conventional microwave plasma reactor (2.45 GHz), with a gas mixture of 3 vol.% methane in excess hydrogen. Each diamond piece was removed from the graphite substrate and pretreated with acid for cleaning and removal of sp^2 residues.

The weight of the diamond substrate was measured in a Sartorius ME5 microbalance, before and after growth, to obtain the mass gain. The use of diamond substrates reduces the error in growth rate measurement because there is no mass loss during growth and by reducing the growth induction time. Each diamond substrate is small enough to have a uniform deposit over its area.

The Arrhenius plot of the natural logarithm of mass growth rate as function of the reciprocal temperature is

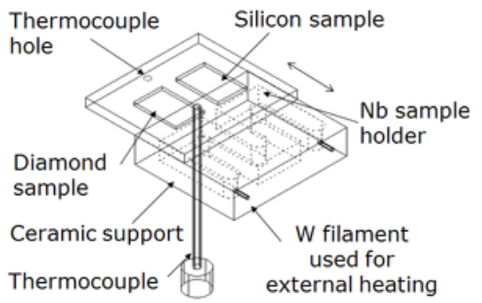

Figure 4. Schematic diagram of the substrate holder used.

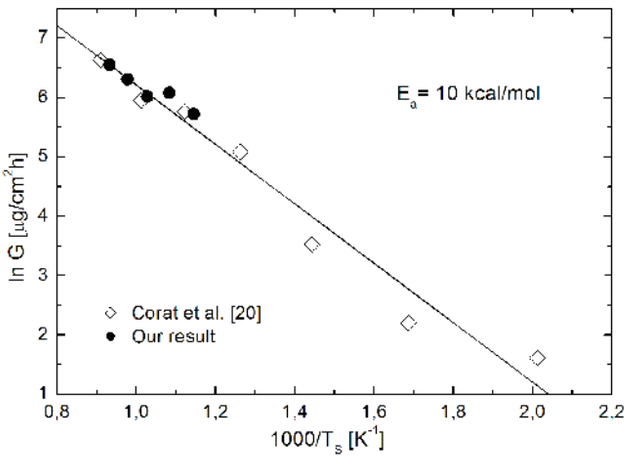

Figure 5. Mass growth rate dependence vs. reciprocal substrate temperature for growth in MCD conditions, as compared to Corat et al. experiments.

compared with the results of Corat et al. [20], obtained by gas phase composed of 1 vol.% CCl_4 in H_2 mixture, as shown in Figure 5. This plot shows the temperature-activated growth, leading to an increasing growth rate as temperature increases. The calculated activation energy was found to be around 10 kcal mol^{-1}. This value confirms the 10 kcal mol^{-1} activation energy of diamond as evaluated by Corat et al. [20], and it is very important to validate the reactor and the method to measure activation energy.

The samples morphology obtained by JEOL JSM-5310 microscope system, Figure 6, presents typical MCD morphology and shows a tendency of grain size increase with the temperature. This tendency is expected in a conventional HFCVD method where the process of diamond growth is thermo-activated.

2.2. Nanostructures of Diamond

Since the number of papers to deal with the substrate temperature of NCD growth is rather limited [17, 18, 21, 70], the base for data comparison is much smaller than for MCD growth. In order to clarify the process, experiments were performed using NCD environment for growth [21].

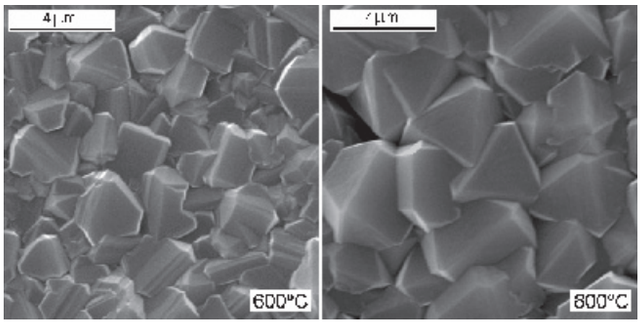

Figure 6. SEM images of the morphology of samples grown to obtain Figure 5.

Films were deposited in the same reactor and under the same conditions as above, described in Section 2.1, except the gas mixture that was 0.5 vol.% methane and 75 vol.% argon balanced with hydrogen, and the typical deposition time that was 12 h. Also, in these experiments, silicon substrates were used for diamond film characterization, and diamond substrates were used for evaluation of activation energy.

The films morphology, Figure 7, shows the top surface in the main image, and the cross section is in the inset. These images reveal a dramatic change in the surface morphology of films grown at different substrate temperatures. The grain size changes from nanometric to micrometric at higher temperatures. The samples grown at 550°C substrate temperatures reveal diamond films with a "ballas-like" morphology and that the films are smooth and continuous and consist of coalescent crystallites that are extremely fine grained. The sectional view does not display the columnar growth typical of MCD, but a granular one. These characteristics are typical of NCD [11]. For the film grown at 650°C the SEM images evidence the initial formation of grains in the (1 0 0) direction, but the "ballas-like" morphology, typical of NCD films, predominates. The images corresponding to the 700 and 750°C substrate temperatures show increasing number of microcrystalline grains. The sectional view reveals that there is a transition from NCD to MCD growth after a long growth period in these samples. This observation indicates that the surface morphology obtained is not typical along the whole growth period but that there is a transition to MCD growth after long periods. This tendency of transition morphology is typically of NCD growth regime, as explained by Williams et al. [85] that above a thickness of around 1 μm the NCD film becomes microcrystalline.

Figure 8 shows the Raman spectra of top surface. It is possible to discriminate the position of the (1) peak in 1150 cm^{-1} assigned to the transpolyacetylene segments at the grain boundaries [65] and typically related with the presence of NCD within the films [18, 66, 86]; (2) first-order Raman line from bulk diamond line at 1332 cm^{-1} (the sp^3-bonded carbon signature); and (3) broad features detected around 1550 cm^{-1} correlated to sp^2-bonded carbon signatures. The characteristic diamond peak at 1332 cm^{-1} is small for the low-temperature samples (550, 600, and 650°C) but increases progressively, conversely the 1150 cm^{-1} decreases with the substrate temperature. These facts confirm the transition from NCD to MCD [66]. The X-ray diffraction of all the samples, Figure 9, detected the diffraction peaks corresponding to the diamond (1 1 1) direction. At 600°C temperature, (2 2 0) and (3 1 1) directions are also shown in the inset. These peaks reveal that all the samples are composed of diamond grains. In Figure 9 it is possible to observe that full width at half maximum (FWHM) of the (1 1 1) peak decreases with the increase of substrate temperature; this behavior when expressed by the well-known Scherer's formula can be used to indicate that the grain size increases with the substrate temperature [22, 87, 88]. This

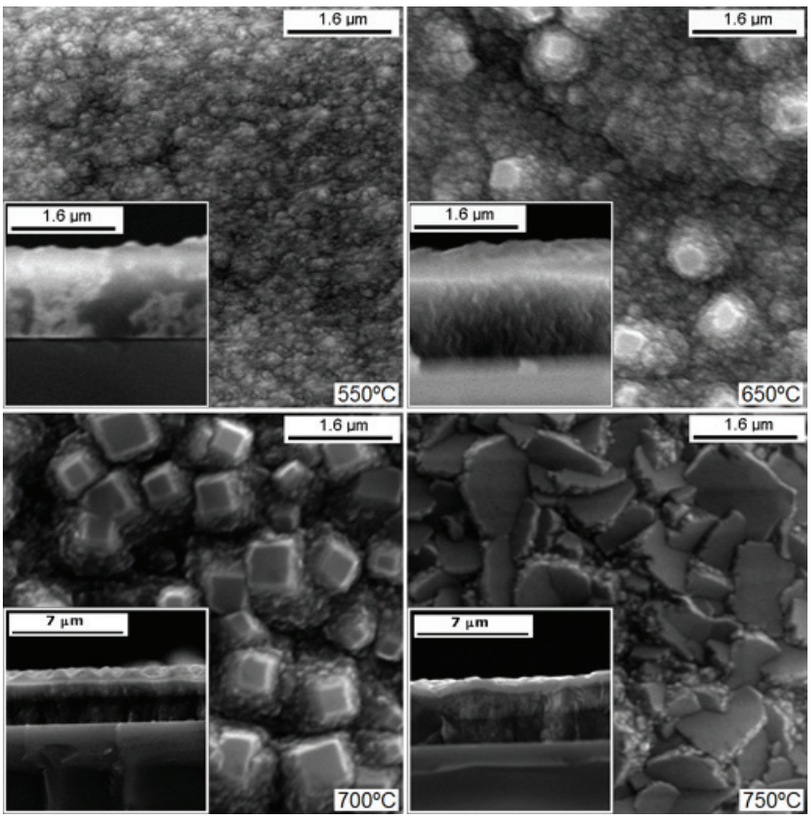

Figure 7. SEM images of the NCD surface grown at different substrate temperatures. The insets show the cross-sectional view.

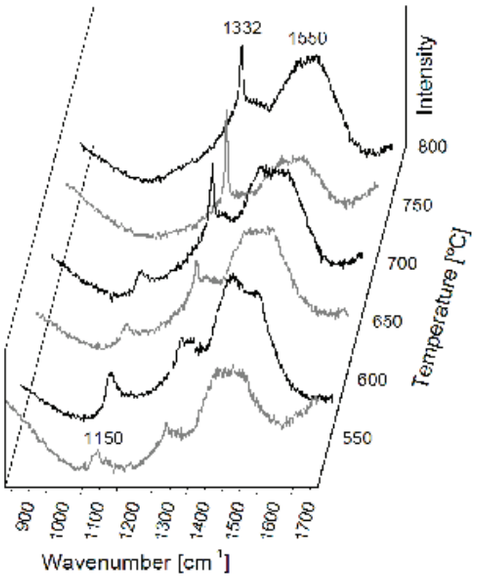

Figure 8. Micro-Raman spectra of NCD deposited at different substrate temperatures.

tendency is expected in HFCVD system where the process of diamond growth is thermo-activated.

The Arrhenius plot of the natural logarithm of growth rate vs. reciprocal temperature is shown in Figure 10. The left axis corresponds to the data for mass growth rate, while the right axis corresponds to the data for thickness growth rate. Mass growth rate was obtained from the diamond substrates, while the thickness growth rate was obtained from the silicon substrates, grown together in each experiment. The linear fitting of the mass growth rate gives activation energy around 10 kcal mol^{-1}. The thickness growth rate is much more scattered around its linear fitting, which gives activation energy around 8 kcal mol^{-1}. The activation energy of 10 kcal mol^{-1} is very similar to the activation energy for MCD growth. Eventhough in these experiments there is a transition from NCD to MCD growth at the highest temperatures, the whole set of activation energy data shows a definite tendency indicating that there is no transition in the growth mechanism. This suggests that the same growth mechanism is responsible for NCD or MCD growths.

Most measurements of activation energy are performed by evaluation of thickness growth rate. This is also the case for the measurements of activation energy for NCD growth shown in the literature [17, 18, 70]. Clearly the measurement of the mass growth rate is a better approach because it measures directly the carbon incorporation independently of the specific mass of the film. The films grown at lower temperatures are clearly observable to be of lower specific mass, which could induce the measurement of lower activation energy with the evaluation of thickness growth rate. Particularly in the case of NCD the high renucleation rate induces a high density of defects that may decrease considerably the specific mass of the film and induce a lower activation energy value. The data on thickness growth rate are very representative of these considerations, not only because the thickness activation energy is smaller, but also because the data are much more scattered owing to the different growth morphologies observed. This point is very critical because the observation of a different activation energy value may induce the conclusion that a different growth mechanism is responsible for the NCD growth. The results shown here

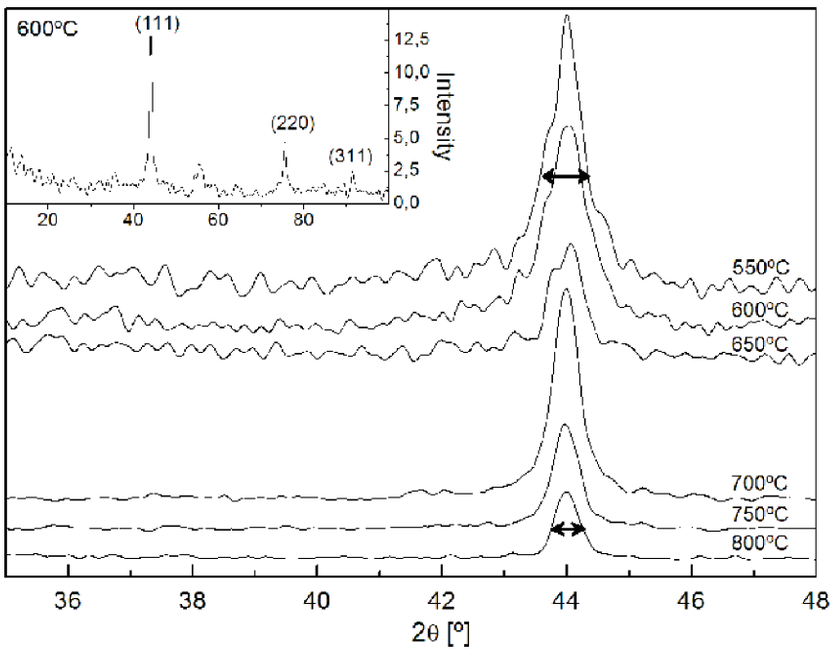

Figure 9. XRD patterns, in the region of the diamond (1 1 1) peak, of NCD films deposited at different substrate temperatures. The inset shows the whole XRD pattern of the 600°C sample.

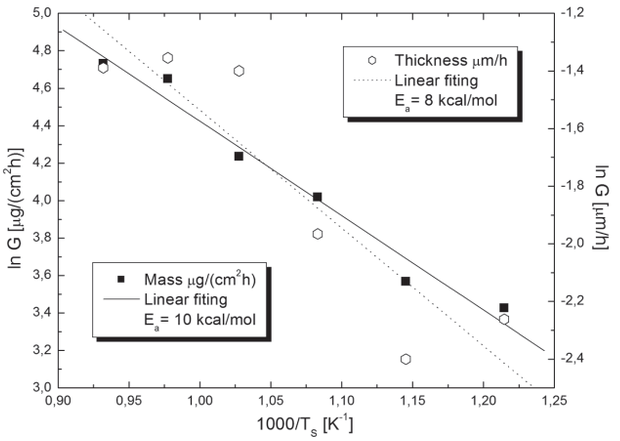

Figure 10. Arrhenius plot of the mass and thickness growth rate vs. reciprocal substrate temperature, for films grown at NCD growth conditions. Reprinted with permission from [21], D. C. Barbosa et al., *J. Nanosci. Nanotechnol.* 9, 3944 (2009). © 2009, American Institute of Physics.

for the activation energy obtained from mass growth rate in a region of transition from NCD to MCD, depending on growth temperature, suggest that the mechanism for NCD growth is the same as the mechanism of MCD growth.

Some references suggest the apparent activation energy for NCD to be 5.85 kcal mol^{-1} [17] and 8.8 kcal mol^{-1} [18], both for growth in MWCVD reactors. They explain these lower activation energies indicating that NCD growth mechanism is different from MCD growth, based on the incorporation of C_2 species [1, 3, 15, 17]. The 10 kcal mol^{-1} obtained here is quite similar to the activation energy for MCD growth, suggesting that there is no change on growth mechanism from MCD to NCD. This result corroborates with a unique MCD and NCD growth mechanism proposed by Paul May, as described in Section 1.3. Further details concerning this work can be found in Ref. [21].

2.3. Ultrananostructures of Diamond

While the number of papers to deal with the substrate temperature of NCD growth is rather limited, in the specific case of UNCD it is quite rare [19, 22]. Further experiments and discussions concerning the gas-phase and surface effects will be necessary to get a unique consensus about this issue. In order to obtain some insights about this subject, a set of experiments were performed taking into account the UNCD growth environment [22]. Films were deposited in the same reactor and under the same conditions as above, described in Sections 2.1 and 2.2, except the gas mixture, that was 1 vol.% methane and 90 vol.% argon balanced with hydrogen, and the typical deposition time that was 8 h.

The samples morphology was analyzed by high-resolution scanning electron microscopy (FEG-SEM) owing to the very small grain formed, as seen in Figure 11. The morphologies of the samples obtained from 550°C to 800°C are very similar, as shown in Figure 11(a), revealing the diamond films with a very fine grain material, with abrupt grain boundaries, grown with a high renucleation rate. It can be seen from Figure 11(a1) that whilst the film shows some contrast, it shows little evidence of crystallinity at this length scale; the inset cross-section image reveals that there is not a columnar structure. These properties and morphology are associated with UNCD grown films [85]. However, in the sample obtained at the highest temperature (850°C), Figure 11(b), the structure is formed by lamellas of graphite with regions where carbon nanotubes and NCD are also developed. This lamellar-like graphite structure was also observed by Mikeheev et al. [89] and called a nanographite structure.

The visible Raman spectrum, obtained at 514.5 nm laser excitation, was used in order to analyze the first- and second-order peaks, as seen in Figure 12. The second-order Raman is used here because it is more appropriate for the detection of most different carbon compounds [65, 90]. From Raman spectrum it is possible to observe the peaks at (1) 1150 cm^{-1}, assigned to the transpolyacetylene segments at the grain boundaries [86] and typically found in diamond nanostructures; (2) 1350 cm^{-1}, the graphite D band; (3) 1580 cm^{-1}, the G band which is the graphite high-frequency E_{2g} first-order mode; (4) 2450 cm^{-1} and 2705 cm^{-1}, referent to graphite G´ band; (5) 2945 cm^{-1}, DG band; and (6) 3244 cm^{-1}, 2D' band [90]. The spectra show that the characteristic G peak increases with the substrate temperature deposition, and in the case of the sample obtained at highest temperature (850°C) the presence of a sharp G' peak confirms the graphitic characteristics noted by the FEG-SEM image.

Figure 13 shows the results from X-ray diffraction analysis. The inset shows the typical diamond (1 1 1), (2 2 0), and (3 1 1) peaks. This X-ray pattern is representative of all the samples and is obtained from a sample grown at 600°C. The observed peaks confirm that these samples are composed of diamond grains. The X-ray diffraction (1 1 1) diamond peak is shown in the main figure at different growth temperatures in the range from 550°C to 800°C. A close observation of these peaks shows a clear broadening with temperature increase. This behavior when expressed by the well-known Scherer's formula can be used to indicate that the grain size decreases with substrate temperature.

In order to provide significant insight into the chemical kinetics involved in the growth surface, the activation energy in this case was also measured. The Arrhenius plot of the natural logarithm of mass growth rate as a function of the reciprocal temperature is shown in Figure 14. This plot shows the temperature-activated growth, leading to an increasing growth rate as temperature increases, as expected for a thermo-activated CVD process. The samples deposited at 700°C, 750°C, and 800°C substrate temperatures presented similar mass growth rate values, around 160 μg (cm^{-2} h); for this only one value was considered for the linear fit. The calculated activation energy was found to be around 6 kcal mol^{-1}. This value is lower than all the values measured for the growth of MCD and NCD films, but is in a good agreement with the results found for nanostructures of diamond reported by some references [17–19]. The authors [3, 15, 17–19] suggest that this lower value is the result of a different growth mechanism for nanostructures of diamond. There is a proposal that for nanostructures growth, the C_2 dimers play a dominant role in renucleation process.

Table 1 is elaborated to directly compare some characteristics of the NCD films shown in Section 2.2 and the

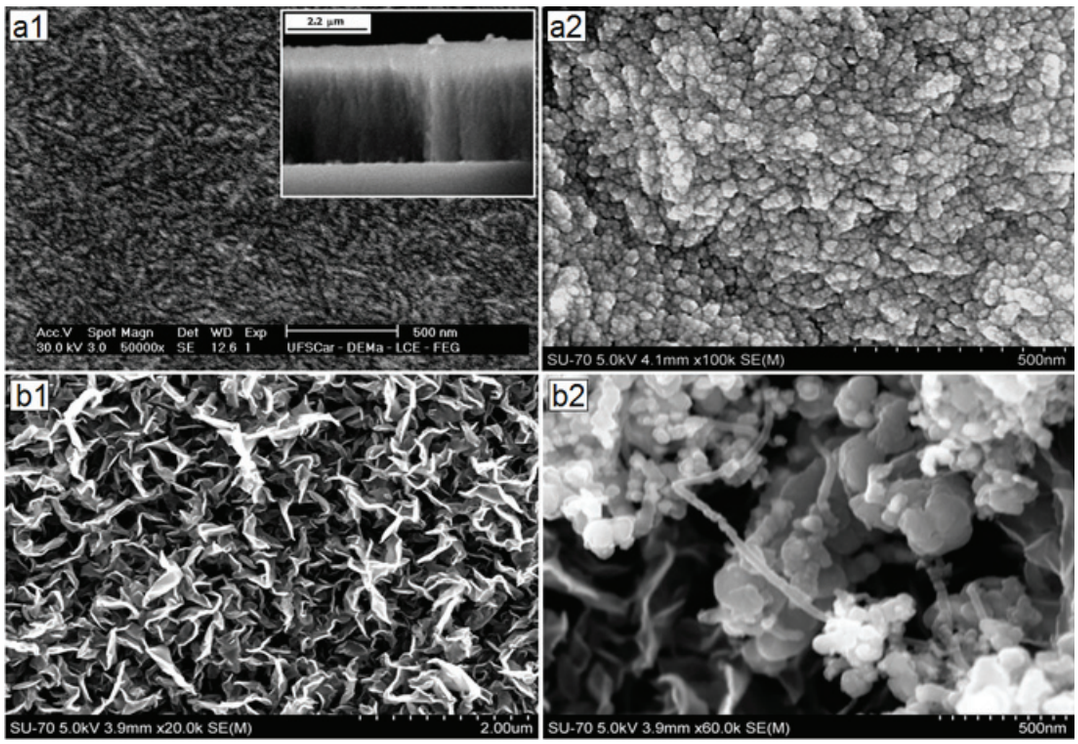

Figure 11. Top view: SEM images of the UNCD grown at the substrate temperature of (a1, a2) 600°C and (b1, b2) 850°C. The inset (a1) shows the cross-sectional view at 600°C substrate temperature.

UNCD samples described in this section. This table shows the results of the (1) mass growth rate, (2) root-mean-square (RMS) surface roughness, and (3) the average grain size measured from FWHM (B) of the (1 1 1) X-ray peak, as obtained by Sherrer′s equation [91]:

$$L = \frac{K\lambda}{B\cos\theta} \tag{2}$$

Here, $K = 0.9$, $\lambda = 1.5406$ Å, and θ is Bragg's angle.

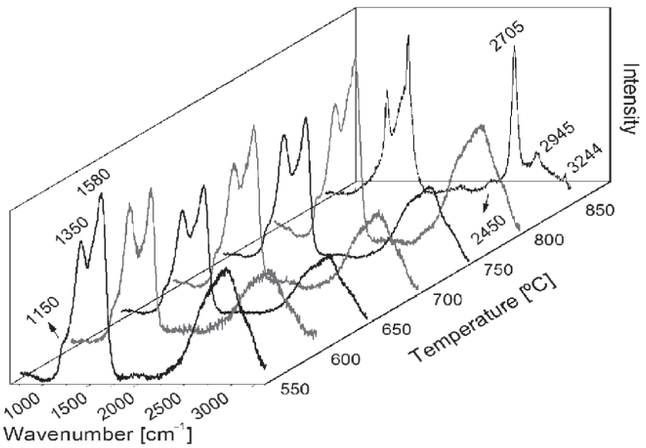

Figure 12. Micro-Raman spectra of UNCD samples grown at different substrate temperatures.

Figure 14, inset, shows the integrated intensity ratio of the D and G band (I_D/I_G), which conventionally represent the degree of order in the clustered aromatic sp^2 phase [90]. It is possible to observe that the relative I_D/I_G ratio increases with the substrate temperature. This behavior suggests that for UNCD there is the formation of nondiamond phase within the film, especially disordered sp^2-hybridized compounds, which are accentuated at higher temperatures. Nonetheless, for NCD this nondiamond phase is suppressed by the increasing substrate temperature. Surface roughness, which depends on the degree of crystallinity in the film, decreases for UNCD, while it increases for NCD at higher temperatures. The calculated grain size for UNCD decreases, while it increases for NCD, with the substrate temperature increase.

The normal behavior of a thermo-activated process is to obtain an increasing grain size if an increasing growth rate is activated. This is the case for NCD, which indicates a normal thermo-activated process. However, for UNCD the tendency is contrary to the expected. This is a key observation for the interpretation of the results because it shows that for UNCD it is not possible to make a direct correlation between the measured activation energy and a simple thermo-activated process.

The other results shown in Table 1 are indicative of a possible explanation for this controversial result. It is known that the defect density in the crystals affects strongly the grain size calculated from the peak broadening of XRD peaks [92, 93]. So, the UNCD behavior of decreasing crystal size suggests that the defect density increases when induced at higher temperatures. This tendency is in good agreement with Raman analyzes that show, for UNCD,

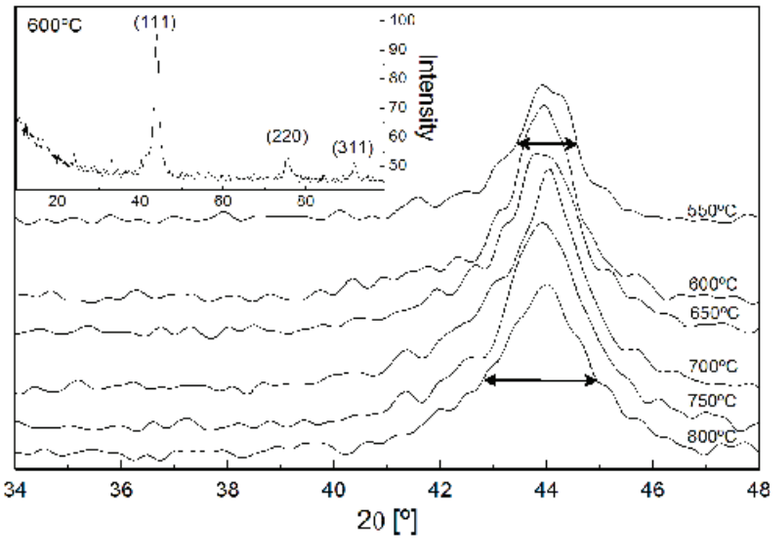

Figure 13. XRD patterns, in the region of the diamond (1 1 1) peak, of UNCD films deposited at different substrate temperatures. The inset shows the whole XRD pattern of the 600°C sample.

the increase of defect density with growth temperature. The I_D/I_G ratios indicate that the higher defect density is directly correlated with the formation of sp^2 phases in the film.

In summary, the techniques present complementary results. Raman analyses show the increase of defect density by an increase in sp^2 phases, while X-ray diffraction analysis shows it on diamond structure itself. The increasing graphitic character of UNCD shown by Raman analysis indicates that the higher competition with sp^2 phase growth is the most probable reason for the increase in defect density, hence decreasing the diamond grain size.

A very interesting result is shown in Figure 15. Both mass and thickness growth rates were measured in these UNCD experiments. The ratio of mass growth rate with thickness growth rate is indicative of the film specific mass, as shown. Specific mass decreases considerably with temperature increase, ranging from values close to diamond specific mass, at low temperature, to values close to graphite specific mass at high temperature.

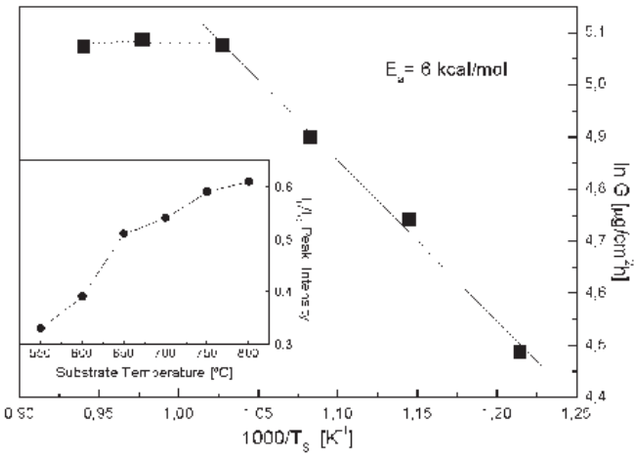

Figure 14. Arrhenius plot of the mass growth rate vs. reciprocal substrate temperature for samples grown at UNCD conditions. The inset shows the relative intensities of the 1350 cm^{-1} (D band) and 1580 cm^{-1} (G band) (I_D/I_G).

Table 1. Comparison of the properties of UNCD and NCD films grown at different substrate temperatures.

Substrate temperature (°C)	UNCD, 90 vol.% argon, 1 vol.% methane, and 9 vol.% hydrogen gas mixture			NCD, 75 vol.% argon, 0.5 vol.% methane, and 24.5 vol.% hydrogen gas mixture		
	Growth rate (μg cm^{-2} h)	Grain size measured by X-ray (nm)	r.m.s. surface roughness (nm)	Growth rate (μg cm^{-2} h)	Grain size measured by X-ray (nm)	r.m.s. surface roughness (nm)
550	88.88	6.74	15.47	30.77	10.85	37.7
600	114.46	6.47	14.36	35.44	12.01	33.4
650	134.09	5.40	12.25	55.57	15.18	79.9
700	160.03	4.93	12.47	121.63	19.33	110.0
750	161.89	4.87	11.53	104.59	19.79	169.0
800	159.44	4.58	12.37	113.49	22.17	318.0

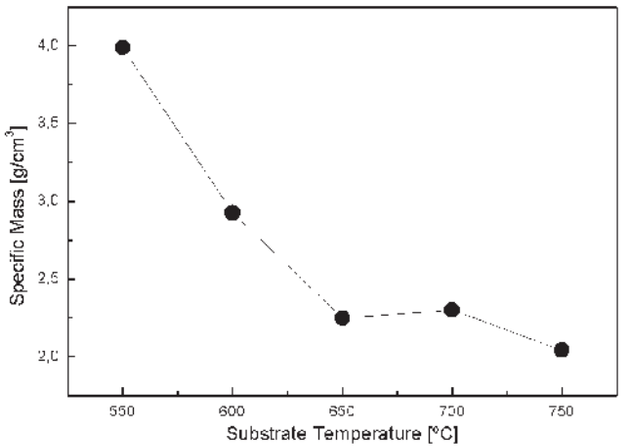

Figure 15. Substrate temperature vs. specific mass, the value changes of diamond value (around 4 g cm^{-3}) and for graphitic value (around 2 g cm^{-3}).

From these observations, Barbosa et al. [22] suggest that the different values of activation energy for MCD, NCD, and UNCD are not necessarily owing to different growth mechanisms. The high competition with the growth of sp^2 phases is the most probable reason for the lower activation energy during the growth of UNCD, and not a different mechanism for the growth of the sp^3 phase.

These observations are in closer agreement with a more recent model proposed by May et al. [14, 47] as described in Section 1.3, which consists of a unique model for any dimensional structure of diamond. They suggest that in the growth of nanostructures many species are present in the activation region, including H, CH_3, C_2H_2, CH_2, CH, C as well as C_2, and several of these species could take place in the growth process, but the CH_3-driven mechanism continues to be the predominant one for conditions where hydrogen concentration is high. However, these experimental results also indicate that only a more complete model, taking into account the competition between sp^3 and sp^2 phases growth, would be able to explain the process of UNCD growth.

3. INFLUENCE OF METHANE CONCENTRATION

The study of the diamond growth rate as a function of temperature at different methane concentrations is very important because it can give significant insights about the gas-phase kinetic. There are many publications that have reported the influence of the methane feed in the gas phase for CVD diamond growth [94–99]. However, for an environment with excess argon content in methane-hydrogen mixtures, ideal for diamond nanostructures growth, the number of publications is still scarce [100]. It is known that the methane concentration in the CVD diamond gas mixture has a strong correlation with the growth rate variation and the film morphology. This occurs for MCD [94, 95] as much as for NCD [100, 101] conditions. In order to examine these correlations some experiments were performed taking into account the UNCD growth. The results of these experiments are compared with the results evaluated by the other authors, which report the diamond nanostructures growth [96, 100, 101]. For this work additional experiments were performed in the same reactor and under the same conditions as above, described in Section 2.3, except the feed gas mixtures, that, here, was 90 vol.% argon with methane concentrations varying at 0.5, 0.25, and 0.125 vol.% and balanced with hydrogen, at a total pressure of 30 Torr. Five straight 125 μm diameter filaments were used, and the distance between the filaments and substrate was of 5 mm. Experiments were performed at different temperatures in the 550–800°C range. Deposition experiments of 24 h were performed for 0.125 vol.% methane concentration and 8 h for the other samples. The samples obtained at 0.125 vol.% methane were deposited with this longer time because it presented a much lower growth rate. Further details of these experiments are presented elsewhere [102].

Experimental results of the Arrhenius plot of thickness growth rate are shown in Figure 16, compared with the data of the other authors. Thickness growth rate was obtained just to perform this comparison, since, as explained in Section 2, the mass growth rate is much better to evaluate the activation energy. It can be seen from this figure that the results obtained are in good agreement with the activation energy and the growth rate for nanostructured diamond films evaluated by the other authors [17, 18, 70]. Two data are clearly shown. The first one concerns activation energies of around 8 kcal mol^{-1} and the second concerns activation energies of around 6 kcal mol^{-1}. The first group, around 8 kcal mol^{-1}, is composed of three different experiments: (1) with 90 vol.% argon, 1 vol.% methane, and 9 vol.% hydrogen gas mixture (the experiment described in Section 2.3); (2) with 90 vol.% argon, 0.5 vol.% methane, and 9.5 vol.% hydrogen gas mixture; and (3) Kulisch et al. [18] experiment obtained by an MWCVD reactor using

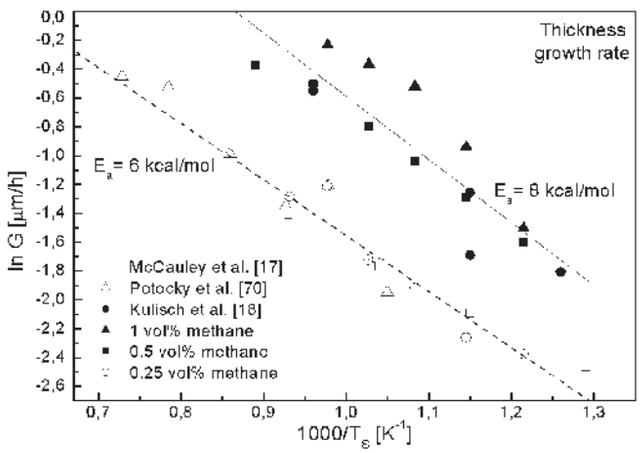

Figure 16. Arrhenius plot comparison of different methane concentrations in the feed gas. The thickness growth rate vs. reciprocal temperature is plotted. The gas mixture used was 90 vol.% argon, methane in excess hydrogen, typical of UNCD growth conditions.

17 vol.% CH_4 and N_2 gas mixture. The second group, of 6 kcal mol^{-1}, is also composed of three different experiments: (1) with 90 vol.% argon, 0.25 vol.% methane, and 9.75 vol.% hydrogen gas mixture; (2) McCauley et al. [17] experiment obtained by an MWCVD reactor using 99 vol.% Ar in CH_4 gas mixtures; and (3) Potocky et al. [70] experiment obtained by a plasma CVD reactor using 5 vol.% CH_4 and H_2 gas mixture. It is impressive that not only the activation energy values but also the growth rate values are so close, considering that completely different gas compositions and growth methods are reported. The only common characteristic is the film morphology, since in all the other cases the growth of diamond nanostructures was reported. Independent of the interpretation the authors have attributed to their data, the similarity of results evaluated for this two groups can be used to indicate a similar tendency for surface growth mechanism.

The Arrhenius plot of the mass growth rate, Figure 17, is also evaluated but now only for the data of this work. Two data groups are found in this graph, one concerns the 0.5 and 1 vol.% methane in feed gas and the other concerns the 0.25 vol.% methane in feed gas. The experiments of the first group, which present 6 kcal mol^{-1} by mass growth rate and 8 kcal mol^{-1} by thickness growth rate, have characteristics of a competition with the growth of nondiamond phases, as explained in Section 2.3. The grain size measured by X-ray diffraction presents decreasing behavior with substrate temperature, the I_D/I_G presents increasing behavior with substrate temperature, and the samples obtained at higher substrate temperatures present graphitic morphology.

The 0.25 vol.% methane experiments, that present 10 kcal mol^{-1} by mass growth rate and present 6 kcal mol^{-1} by thickness growth rate, have characteristics of diamond preferential growth. The grain size measured by X-ray diffraction presents increasing behavior with substrate temperature, the I_D/I_G presents decreasing behavior with substrate temperature, and the samples at higher substrate temperatures (more than 750°C) show preferential MCD morphology.

From this comparison results, it is clear that the measurement of the mass growth rate is a better approach in order to identify the preferential growth regimen that occurs in an argon-rich environment for CVD diamond growth: 10 kcal mol^{-1} corresponds to a regimen of diamond sp^3 preferential growth

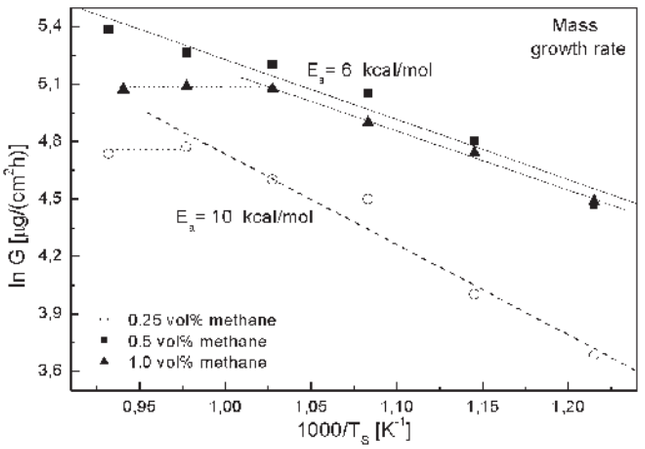

Figure 17. Arrhenius comparison plot of different methane feeds. The mass growth rate vs. reciprocal substrate temperature is plotted. The gas mixture used was 90 vol.% argon, methane in excess hydrogen, typical of UNCD growth conditions.

and 6 kcal mol^{-1} is obtained if there is a high competition with the growth of nondiamond phases. Finally, these experiments show that in the preferential diamond growth regimen the same activation energy around 10 kcal mol^{-1} is obtained, which indicates the methyl radical-driven mechanism.

The competition between the diamond and the nondiamond phases is also observed with the variation of methane content in the feed [96, 100, 101], as demonstrated in Figure 18 for experiments performed at 750°C. This figure reveals a dramatic change in the surface morphology of films obtained at different methane concentrations. The samples change from faceted microstructures of diamond, pass through ballas-like morphology, and finally come to lamellar graphitic morphology.

From the Raman spectrum, Figure 19, it is also possible to observe this dramatic change. It can be observed that the characteristic first-order Raman line from bulk diamond at 1332 cm^{-1} is much intense in 0.25 vol.% methane experiment, shows discreet presence in 0.5 vol.% methane experiment, is occulted by other bands present in the 1 vol.% methane experiment, and is not present in the 1.5

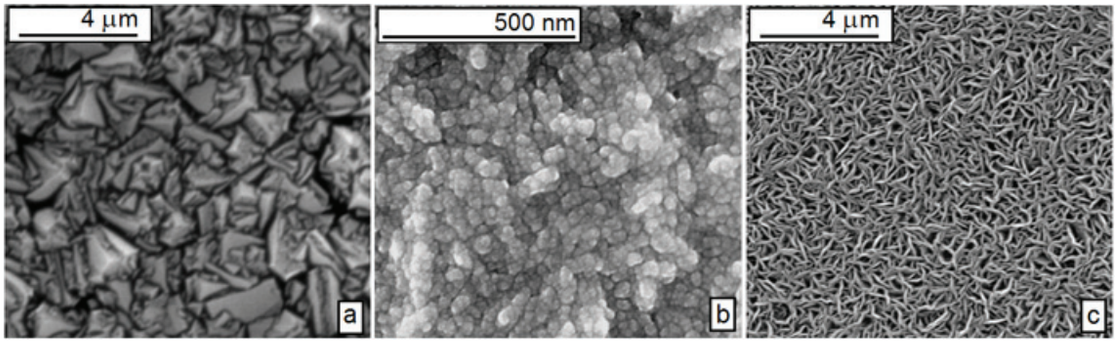

Figure 18. Top-view SEM images of the films grown at 750°C substrate temperature and 90 vol.% argon with (a) 0.25, (b) 1, and (c) 2 vol.% methane in hydrogen gas mixture.

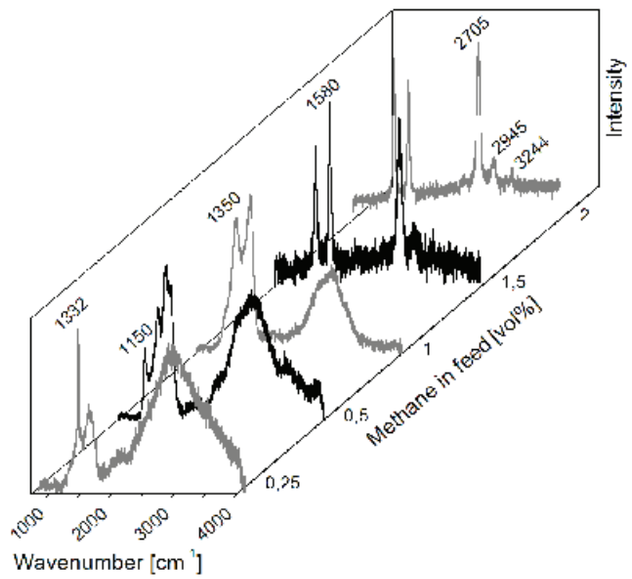

Figure 19. Micro-Raman spectra of the samples obtained at different methane concentrations and 90 vol.% argon in hydrogen. Samples were grown at 750°C substrate temperature

and 2 vol.% methane experiments. Meanwhile, the G band (1580 cm^{-1}) and D band (1350 cm^{-1}), both correspond to the presence of sp^2 phases on the surface and become evident from 1 to 2 vol.% methane experiment. The 2705 cm^{-1} G' peak, 2945 cm^{-1} DG peak, and 3244 cm^{-1} 2D' peak confirm that 1.5 and 2 vol.% methane are samples composed of graphitic structure.

Further analysis, which is very important in this chapter, is obtained by plotting the growth rate as function of methane concentration in feed gas, at 750°C, but with the explicit indication of resulting morphology and of the obtained activation energy. This is plotted for thickness growth rate in Figure 20 and for mass growth rate in Figure 21. The typical morphologies are faceted (typical of MCD), ballas-like (typical of UNCD), and graphitic. The activation energies were obtained from the corresponding experiments with variation of substrate temperature at the given methane concentration in the feed gas. Each curve shows a maximum in the growth rate at a transition in film morphology.

From Figure 20 it is possible to see that (1) while diamond structures are obtained (MCD and UNCD), the growth rate has a positive slope, leading to higher value of thickness growth rate with the methane feed; (2) the activation energy values do not present drastic changes, the calculated values were around 6 and 8 kcal mol^{-1}, as shown in Figure 16; (3) the activation energy values found are lower than values found from a typical MCD deposition (approximately 10 kcal mol^{-1}); and (4) the transition to a negative slope of growth rate is abrupt and occurs only when nanographite is the preferential morphology observed on the sample.

From Figure 21 it is possible to observe that (1) the mass growth rate increases (or there is a positive slope) with methane concentration in feed gas only while faceted morphology is seen on the sample; (2) there is a drastic change in the activation energy, from 10 to 6 kcal mol^{-1}, as also shown in Figure 17, which accompanies the morphology change from faceted to ballas-like; (3) the activation energy values calculated for the samples obtained at lower methane concentrations (0.25 vol.%) agree with the value for typical MCD growth (10 kcal mol^{-1}); (4) the activation energy values calculated for the samples obtained at 0.5 and 1 vol.% methane agree with the values found for typical UNCD growth (6 kcal mol^{-1}); (5) the slope transition occurs when the samples show UNCD preferential morphology; (6) the mass growth rate has a linear, smooth, and decreasing behavior (a negative slope) after UNCD morphology appears; and (7) continues with this same negative slope even after the nanographite becomes the preferential morphology seen on the sample.

Very interesting at these graphs, Figures 20 and 21, are the differences in observed transition from the positive to

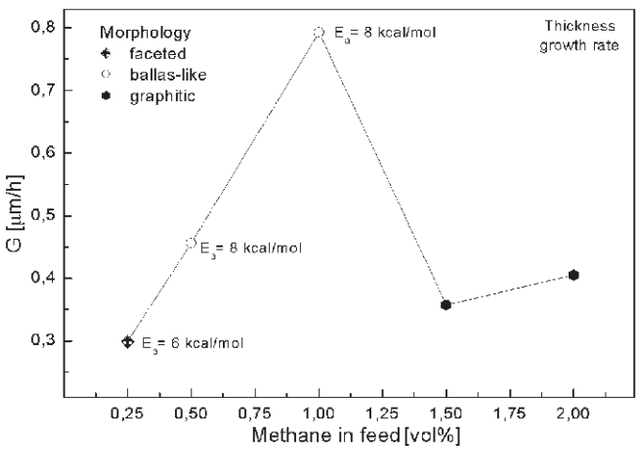

Figure 20. Concentration of methane feed vs. thickness growth rate for samples shown in Figure 16.

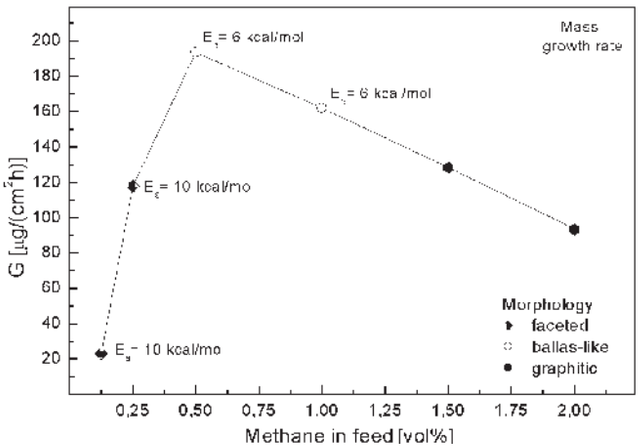

Figure 21. Concentration of methane feed vs. mass growth rate for the same samples of Figure 17 .

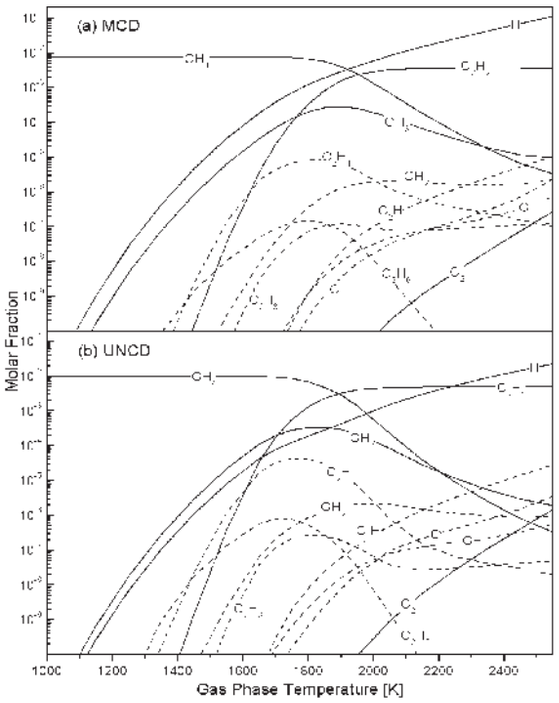

Figure 22. Calculated gas-phase composition as a function of dissociation temperature: (a) MCD conditions, consisting of 1 vol.% methane in hydrogen and (b) UNCD conditions, consisting of 90 vol.% argon and 1 vol.% methane in 9 vol.% hydrogen. All calculations were performed at the same pressure value of 30 Torr.

negative slope. It is worth to recall. For thickness growth rate it occurs in the transition from UNCD to nanographite and for mass growth rate it occurs in the transition from MCD to UNCD morphologies. From Figure 20 it is possible to see an abrupt transition on thickness growth rate that occurs only when nanographite morphology is predominant.

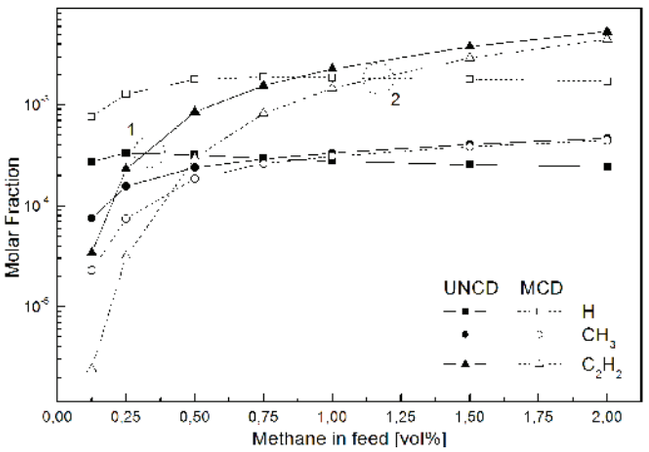

Figure 23. Calculated molar fraction as a function of methane concentration, considering 1850 K gas temperature, 30 Torr of pressure, and gas mixtures of (MCD) methane in excess hydrogen and (UNCD) 90 vol.% argon and methane-hydrogen.

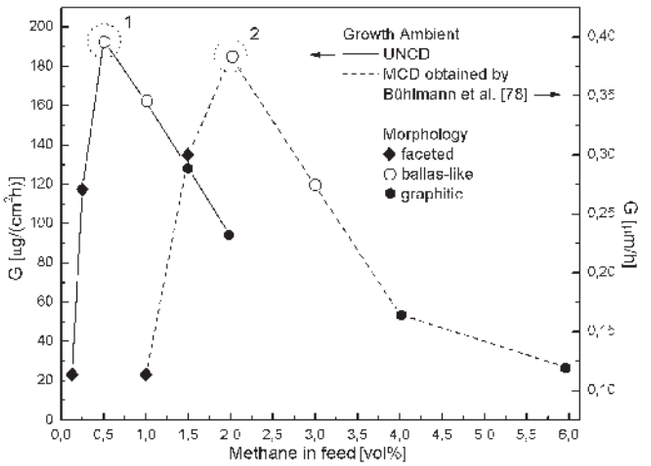

Figure 24. Comparison of the mass growth rate obtained for UNCD vs. MCD growth conditions. The UNCD is correspondent to Figure 21 and the MCD data were extracted from Ref. [94], and were obtained at 950°C substrate temperature in MWCVD reactor. The authors of Ref. [94] calculated the growth rate from weight differences of the substrate before and after deposition, assuming a constant density for diamond.

However, the same morphology transition border presents a smooth behavior on mass growth rate of Figure 21. This same smooth behavior for mass growth rate in transition to a graphitic morphology is also observed by Bühlmann et al. [94] in an environment without argon, at 950°C substrate temperature and using MWCVD method. The main difference is that in the Bühlmann case this morphology transition occurs at approximately 2 vol.% methane.

These differences in transition border, observed by comparison of Figures 20 and 21, are most probably observable because the mass growth rate is more efficient in identifying the high sp^2/sp^3 competition in this regimen. Mass growth rate is already able to discern the increasing sp^2 content in the transition to UNCD growth.

Finally, these results suggest that methane concentration in feed gas of argon-rich CVD diamond growth, ideal for growth of diamond nanostructures, alters the gas-phase kinetic, modifying the activation energy and, as proposed by other authors in a environment without argon [95, 96], exerts a strong correlation between the growth rate variation and morphology. In such case, the mass growth rate morphology transition border is in close agreement with the results obtained at environment without argon [94, 95], as also shown in Figure 24. Figure 24 will be further discussed in the next sections with the help of some model calculations.

4. COMPARISON BETWEEN EXPERIMENTAL AND THEORETICAL STUDIES

Theoretical models for diamond nanostructures growth have been a subject of great interest in the scientific community [14, 16, 47, 101]. Nowadays, the most representative

study is owing to May and Mankelevich [14, 47, 101], which proposed a model based on competition between H atoms, CH_3 radicals, and other C_1 radical species reacting with dangling bonds on the diamond surface. This study suggests that growth of all types of diamond, UNCD, NCD, MCD, or single diamond crystal (SCD) can broadly be explained in a unique model. In this model, the knowledge of the gas-phase concentrations near the growing diamond surface is used to estimate the growth rate and the average crystal size during CVD diamond growth, and thereby to predict the film morphology [47]. This work is very important because it is in close agreement with the experimental results obtained by the scientific community that indicate that micro- and nanodiamond structures are obtained in the same growth mechanism, independently of the gaseous phase, as explained in Section 3. However, May and Mankelevich [14] did not discuss the relationship between their theoretical calculation with the experimental results dependence on activation energy and methane concentrations. Therefore, in order to obtain insights of this relationship with the experimental data discussed in Sections 2 and 3, a simulation model is evaluated here.

To clarify the differences between the gaseous phase environment without argon and that is argon-rich, the CHEMKIN package [103] was used for the theoretical simulation. The simulation developed here assumes one-dimensional flow. Thus, the gas-phase temperature and species concentrations depend only on the distance between the substrate and the filaments; consider 5 mm in this case. Each reported experimental condition of pressure, temperature, and mass flow rate were used to determine the residence time. The gas-phase kinetic mechanism is based on [104] 25 species produced, and consumed 57 elementary chemical reactions. The gas phase is considered with a total pressure of 30 Torr.

Figure 22 shows the calculated molar fraction vs. gas-phase temperature obtained for (a) a gas-phase environment with 99 vol.% of hydrogen and 1 vol.% of methane, typically used for MCD growth and for (b) a gas-phase environment with 90 vol.% argon, 1 vol.% methane and 9 vol.% hydrogen, typically used for UNCD growth. This figure was elaborated to compare the main species molar fraction (H atomic, CHx, C_2Hy, C, and C_2) in environment favorable for the growth of MCD and UNCD structures, respectively. This comparison is very important because, as discussed in Section 1.2, the quality of the diamond film depends on the identity of the main growth species. For example: an environment containing CH_4 and CH_3 is much more effective for growing diamond films than one containing C_2H_2 [39–42], the quality of the diamond film is poor in an environment rich of C_2H_2 species [39–41], the substrate adsorption of the C_2Hy gaseous phase species is probably responsible for most of the nondiamond carbon formed [39, 64, 105, 106], C_2H_2 concentration has no correlation with diamond growth kinetics [39, 42], and CH_3 concentration has a strong relationship with diamond growth kinetics [36, 38].

The most interesting fact of the calculations shown in Figure 22 is the molar fraction of the atomic hydrogen, which for MCD conditions, Figure 22(a) , is higher than hydrocarbon growth species, and for UNCD conditions, Figure 22(b), it is lower than CH_3 and C_2H_2 species. In the case of MCD deposition the molar fraction of atomic hydrogen is sufficient to react with the gaseous phase and come to substrate surface to stabilize the diamond clusters and to etch nondiamond carbon formed on the substrate during deposition. This behavior confirms the preferential diamond growth phase observed experimentally in Section 2.1, with the 10 kcal mol^{-1} value for activation energy.

However, for UNCD conditions the molar fraction of atomic hydrogen is lower than C_2H_2, in the range of 1700–2250 K gas-phase temperature. Thus, in the UNCD conditions probably the atomic hydrogen molar fraction is not sufficient for etching the nondiamond phase promoted by the supersaturated C_2H_2 condition. Probably this specific growth environment is responsible for lower (6 kcal mol^{-1}) activation energy measured by HFCVD and for the high competition with the growth of nondiamond phases, observed by the experimental result evaluated in Section 2.3.

Another important aspect, which can be seen in Figure 22(b), is the transition point between the C_2H_2 and the atomic H molar fractions around approximately 2250 K gas-phase temperature. Above 2250 K atomic H molar fraction supersedes the hydrocarbon species. This behavior may explain the differences in growth kinetics for diamond nanostructures deposited in MWCVD and HFCVD, as observed in the literature [47]. It is well known that for HFCVD reactor the gas-phase temperature expected is in the range of 1000–2200 K [107], while in the case of MWCVD reactor the expected gas-phase temperature is higher than 2400 K. Probably this special condition for MWCVD environment is responsible for the C_2 and CH species experimentally found by many works [3, 15–17, 60, 63, 93].

Therefore, there is a delicate balance between the molar fractions of CH_3, C_2H_2, H, and the other gas-phase species in the CVD environment that probably determine the preferential growth phase and hence the film morphology. To further compare the theoretical calculations with experimental results, which are indispensable in other to obtain insights about the chemical-physical kinetics that occurs during diamond deposition, the simulation graph of Figure 23 was obtained. It shows the calculated H, CH_3, and C_2H_2 molar fractions vs. methane concentration in the feed gas. This calculus was obtained in an environment at 1850 K gas temperature, 30 Torr pressure, and gas mixture of (MCD conditions) methane and hydrogen and (UNCD conditions) 90 vol.% argon and methane-hydrogen. The same conditions of experiments are described in Section 3. These calculated molar fraction distributions are in complete agreement with the theoretical results obtained by Dandy and Coltrin [97] for MCD conditions and by May and Mankelevich [101] for UNCD conditions. Likewise, the molar fraction transition where C_2H_2 curve crosses the atomic hydrogen molar fraction, areas 1 and 2 shown in Figure 23 , is also observed by Refs. [101] (Fig. 7 of *J. Appl. Phys.* 100, 024301, 2006) and [97] (Fig. 4 of *J. Appl. Phys.* 76, 3102, 1994), respectively.

The experimental graph of Figure 24 shows the results obtained for UNCD conditions, described in more detail by Figure 19, and the experimental results obtained by Bühlmann et al. [94] for MCD conditions, at 950°C gas temperature and MWCVD reactor. Both of these experimental

results were evaluated by the mass growth rate. The MCD results are given in the units of $\mu m\ h^{-1}$ because the authors [94] calculated the growth rate from weight differences of silicon substrate before and after deposition, but converted to thickness growth rate by assuming a constant density for diamond film.

From Figure 23 it is possible to see that the calculated molar fractions of CH_3 and C_2H_2 for UNCD deposition are higher than the same species for MCD deposition, especially C_2H_2. It is commonly reported in the literature [63] that in the case of UNCD deposition the various hydrocarbon species participate in the formation of film. However, Figure 23 shows that the two most probable precursors for diamond growth have similar or even higher molar fractions than in MCD growth conditions. The really important difference observed in Figure 23 is the much smaller atomic hydrogen molar fraction in the case of UNCD growth conditions.

Important points to remark are regions 1 and 2 marked in Figure 23. Until approximately 0.32 and 1.25 vol.% methane in feed gas, the molar fraction of atomic hydrogen for UNCD and MCD deposition, respectively, are higher than the respective C_2H_2 molar fractions. This supersaturated atomic hydrogen gas mixture condition is expected in a preferential diamond growth environment. Above these methane contents in the feed gas the C_2H_2 molar fraction becomes the most supersaturated specie in the respective environment. Above around areas 1 and 2 in Figure 23, a nondiamond preferential growth environment is expected, respectively, for UNCD and MCD.

Also in the experimental figure 24, two regions, 1 and 2, are marked. They represent the transition region where the slope of growth rate changes from positive to negative and the film morphology changes from faceted grains to ballas-like. In the case of UNCD growth (region 1), it is also the transition region of the activation energy values, which changes from 10 to 6 $kcal\ mol^{-1}$, as shown in more detail in Figure 21. For the case of the MCD data shown in Figure 24, the activation energy data are not available from Bühlmann et al. [94].

A simple examination of the methane content in the feed gas in both the figures (Figs. 23 and 24) indicates that regions 1 and 2 in the respective figures are somewhat correlated. The transition areas observed in Figure 23 concern the supersaturation of C_2H_2 in the environment, and the transition areas observed in Figure 24 concern the changes in the morphology and the activation energy values. It is widely accepted that the C_2H_2 supersaturation induces the formation of sp^2 phases responsible for ballas-like growth. For MCD growth these conditions are very well known and ballas-like growth is obtained at relatively high methane concentrations, typically larger than 2 vol.%, as is the case for the data of Bühlmann et al. The main benefit of this comparison is to observe that a very similar result is observed for UNCD growth, but at much lower methane content. Region 1 of Figure 23 correlates this transition with the much smaller atomic H molar fraction obtained for UNCD conditions.

It is important to notice that this correlation of regions 1 and 2 in Figures 23 and 24 was only perceived owing to the measurement of the mass growth rate, instead of the thickness growth rate. The thickness growth rate would show the change in the growth rate slope only for much higher methane concentration, in the transition to nanographite growth, as already seen in Figure 20 . The triple coincidence of the transitions on growth rate slope, morphology changes (from faceted to ballas-like), and activation energy brought special attention to this point.

Therefore, these comparisons indicate that independent of the gaseous phase, without argon or argon-rich, the diamond growth mechanism is most probably unique. In both the cases, faceted diamond crystals are obtained if there is an atomic H supersaturation, nanostructures of diamond can be grown in an environment where there is a high competition for sp^2 growth owing to the relative increase of C_2H_2 molar fraction, and graphitization is observed for much higher C_2H_2 content in the gas phase.

5. CONCLUSIONS

NCD shows a great promise for use in structural and device applications in which enhanced mechanical and physical properties are required. Substantial progress has been made in the development, processing, and nanostructural aspects of diamonds over the recent years. This chapter provided several review aspects of this diamond nanostructure growth environment. The necessary condition for diamond growth to occur, the physical and chemical aspects necessary for the diamond growth environment, the complex chemical reaction processes involved in this system, and an investigation of the main hydrocarbon growth precursors species are evaluated here.

The importance of the atomic hydrogen in diamond growth environment is discussed and a review about the influence of the inert gas addition on this diamond environment is done. This review is very important to the achievement of understanding of the factors that control the diamond crystal size. The role that argon addition plays in HFCVD system is also discussed. From this it is shown that changing the hydrogen content by argon decreases the diamond grain size, but also increases the defect density in the structure of the film obtained.

To illuminate the explicit function of argon addition, a review and comparison of experiments with and without argon is done. First, the influence of the substrate temperature is analyzed for hydrogen and methane environment, ideal for growth of microstructures of diamond, and second for hydrogen, methane, and argon environment, ideal for growth of nanostructures of diamond, and finally for hydrogen, methane, and argon-rich environment, ideal for growth of ultrananostructures of diamond. From these review and experiments it is proposed that argon addition causes an increase in the competition of sp^2 and sp^3 phases on the diamond growth surface. This high competition is appointed as the reason for lower activation energy found for UNCD deposition. Not only a new growth mechanism but also the influence of the competition for growth of two different phases is the most probable reason for the lower activation energy. Despite the observed competition of sp^2 growth, the UNCD growth at optimized conditions

produces diamond of very good crystalline quality with little sp^2 phase content.

Methane concentration in feed gas influence is also analyzed. The review and experiments indicate that both high methane concentration as well as argon addition have the effect on the formatiDon of diamond nanostructures and graphite. Experiments evaluated here show that increasing methane in feed gas of argon-rich environment alters the gas-phase kinetic, modifying the activation energy, and as reviewed, exerts a strong correlation between the growth rate slope and morphology.

Besides, theoretical models, leading to account an environment with and without argon, are reviewed and evaluated. The review and simulation proposed here show that the delicate balance between the molar fractions of CH_3, C_2H_2, and H species in the CVD environment determines the preferential growth phase morphology (faceted, ballas-like, and graphitic), and hence the diamond grain size. Finally, a comparison of theoretical and experimental results, obtained here and revised from the literature, indicate that (1) independent of the gaseous phase, without argon or argon-rich, the diamond growth mechanism is unique; and (2) the high quantities of the C_2H_2 molar fraction in the gas phase are first responsible for the high competition with the growth of sp^2 phases that result in UNCD growth and stimulate the graphitization process observed with increasing methane concentration.

These observations are very important for modeling of the process. Recent models are based on the principle that nanodiamonds are a result of diamond growth with a high renucleation rate. The review of the activation energy measurements indicates that this is true for NCD growth, but all the evidences show that this is not the case for UNCD growth. Probably a model considering the competition between a diamond growth mechanism with a sp^2 growth mechanism would give better results for UNCD growth. A complete unified model would observe the transitions from MCD to NCD, from NCD to UNCD, and from UNCD to nanographite.

Essential for most observations shown here was the perception that mass growth rate instead of thickness growth rate should be used. Mass growth rate is much more sensitive to the variation of the growth phases. This is very important for such a transitional region. It is clearly shown here that the common sense assumption of uniform film deposition with a constant specific mass is not correct. The measurement of mass growth rate clearly and naturally shows some important aspects of the CVD diamond growth process. It clarifies that many of the variations in growth dependence with temperature or methane concentration are not owing to a variation of the growth process, but simply a variation of film specific mass owing to the competition with the growth of the sp^2 phases.

Obviously, many more experiments and much more data will be needed to resolve all these issues, mainly because actually the title of this chapter is an assumption of intense discussion in the scientific community. The developments in diamond nanostructures described here have profound consequence for the usefulness of diamond as a material.

ACKNOWLEDGMENTS

We are grateful to CAPES (Coordenação de Aperfeiçoamento de Pessoal de Nível Superior) and FAPESP (Fundação de Amparo a Pesquisa do Estado de São Paulo) (Proc. #07/00013–4) for the financial support of this work, Ilda and Renata for precisely weighting the samples, and all the members of the INPE diamond group (DIMARE) for useful discussions and laboratories assistance.

REFERENCES

1. O. A. Shenderova and D. M. Gruen, "Ultrananocrystalline Diamond Synthesis, Properties, and Applications," Norwich, NY: William Andrew Publishing, 2006.
2. D. Das and R. N. Singh, *Int. Mater. Rev.* 52, 29 (2007).
3. D. M. Gruen, *Annu. Rev. Mater. Sci.* 29, 211 (1999).
4. A. R. Krauss, O. Auciello, D. M. Gruen, A. Jayatissa, A. Sumant, J. Tucek, D. C. Manicini, et al., *Diamond Relat. Mater.* 10, 1952 (2001).
5. E. C. Almeida, A. F. Azevedo, M. R. Baldan, N. A. Braga, J. M. Rosolen, and N.G.Ferreira, *Chem. Phys. Lett.* 438, 47 (2007).
6. A. V. Sumant, A. R. Krauss, D. M. Gruen, O. Auciello, A. Erdemir, M. Williams, A. F. Artiles, and W. Adams, *Tribol. Trans.* 48, 24 (2005).
7. O. A. Williams, *Semicond. Sci. Technol.* 21, R49 (2006).
8. S. Bhattacharyya, O. Auciello, J. Birrell, J. A. Carlisle, L. A. Curtiss, A. N. Goyette, et al., *Appl. Phys. Lett.* 79, 1441 (2001).
9. O. A. Williams, S. Curat, J. E. Gerbi, D. M. Gruen, and R. B. Jackman, *Appl. Phys. Lett.* 85, 1680 (2004).
10. P. Bajaj, D. Akin, A. Gupta, D. Sherman, B. Shi, O. Auciello, and R. Bashir, *Biomed. Microdev.* 9, 787 (2007).
11. Y. F. Zhang, F. Zhang, Q. J. Gao, X. F. Peng, and Z. D. Lin, *Diamond Relat. Mater.* 10, 1523 (2001).
12. A. N. Jones, W. Ahmed, I. U. Hassan, C. A. Rego, H. Sein, M. Amar, and M. J. Jackson, *J. Phys. Cond. Matt.* 45, S2969 (2003).
13. J. Grifin and P. C. Ray, *Nanotechnology* 17, 1225 (2006).
14. P. W. May, M. N. Ashfold, and Y. A. Mankelevich, *J. Appl. Phys.* 101, 053115 (2007).
15. P. C. Redfern, D. A. Horner, L. A. Curtiss, and D. M. Gruen, *J. Phys. Chem.* 100, 11654 (1996).
16. A. Hoffman, I. Gouzman, and S. Michaelson, *Thin Solid Films* 515, 14 (2006).
17. T. G. Mccauley, D. M. Gruen, and A. R. Krauss, *Appl. Phys. Lett.* 73, 1646 (1998).
18. W. Kulisch, C. Popov, S. Boycheva, M. Jelinek, P. N. Gibson, and V. Vorlicek, *Surf. Coat. Technol.* 200, 4731 (2006).
19. X. Xiao, J. Birrel, J. E. Gerbi, O. Auciello, and J. A. Carlisle, *J. Appl. Phys.* 96, 2232 (2004).
20. E. J. Corat, R. C. Barros, V. J. Trava-Airoldi, N. G. Ferreira, N. F. Leite, and K. Iha, *Diamond Relat. Mater.* 6, 1172 (1997).
21. D. C. Barbosa, L. L. Melo, V. J. Trava-Airoldi, and E. J. Corat, *J. Nanosci. Nanotechnol.* 9, 3944 (2009).
22. D. C. Barbosa, F. A. Almeida, R. F. Silva, N. G. Ferreira, V. J. Trava-Airoldi, and E. J. Corat, *Diamond Relat. Mater.* [in press], doi: 10.1016/j.diamond.2009.05.002.
23. H. Liu and D. S. Dandy, "Diamond Chemical Vapor Deposition," New Jersey, USA: Noyes Publications, 1995.
24. F. P. Bundy, W. A. Bassett, M. S. Weathers, R. J. Hemley, H. K. Mao, and A. F. Goncharov, *Carbon* 34, 141 (1996).
25. S. Matsumoto, Y. Sato, M. Kamo, and N. Setaka, *Jpn. J. Appl. Phys.* 21, L183 (1982).
26. R. F. Davis, "Diamond Films and Coatings," New Jersey, USA: Noyes Publications, 1993.
27. J. Singh, *J. Mater. Sci.* 29, 2761 (1994).
28. P. W. May, Phil. *Trans. R. Soc. Lond. A* 358, 473 (2000).

29. L. Schafer, M. Hofer, and R. Kroger, *Thin Solid Films* 515, 1017 (2006).
30. A. Amorim, P. A. P. Nascente, V. J. Trava-Airoldi, E. J. Corat, A. R. Alves, and J. R. Moro, *Vacuum* 83, 1054 (2009).
31. P. W. May, J. A. Smith, and Y. A. Mankelevich, *Diamond Relat. Mater.* 15, 345 (2006).
32. F. G. Celii and J. E. Butler, *Annu. Rev. Phys. Chem.* 42, 643 (1991).
33. J. C. Angus, Y. Wang, and M. Sunkara, *Annu. Rev. Mater. Sci.* 21, 221 (1991).
34. K. E. Spear and J. P. Dismukes, "Synthetic Diamond: Emerging CVD Science and Technology," New York: John Wiley & Sons, 1994.
35. M. H. Nazareth and A. J. Neves, "Properties, Growth and Applications of Diamond," London, United Kingdom: INSPEC, The Institution of Electrical Engineers, 2001.
36. D. G. Goodwin, *Appl. Phys. Lett.* 59, 277 (1991).
37. S. J. Harris, *Appl. Phys. Lett.* 56, 2298 (1990).
38. E. J. Corat and D. G. Goodwin, *J. Appl. Phys.* 74, 2021 (1993).
39. S. J. Harris and L. R. Martin, *J. Mater. Res.* 5, 2313 (1990).
40. L. R. Martin and M. W. Hill, *Appl. Phys. Lett.* 55, 2248 (1989).
41. L. R. Martin and M. W. Hill, *J. Mater. Sci. Lett.* 9, 621 (1990).
42. S. J. Harris and A. M. Weiner, *Thin Solid Films* 212, 201 (1992).
43. S. J. Harris and D. G. Goodwin, *J. Phys. Chem.* 97, 23 (1993).
44. D. G. Goodwin, *J. Appl. Phys.* 74, 6888 (1993).
45. D. G. Goodwin and G. G. Gavillet, *J. Appl. Phys.* 68, 6393 (1990).
46. A. S. Barnard, P. Bath, S. P. Russo, and I. K. Snook, *Mol. Simul.* 30, 1 (2004).
47. P. W. May and Y. A. Mankelevich, *J. Phys. Chem. C* 112, 12432 (2008).
48. W. A. Yarbrough and R. Messier, *Science* 247, 688 (1990).
49. C. Liu, X. Xiao, J. Wang, B. Shi, V. P. Adiga, R. W. Carpick, J. A. Carlisle, and O. Auciello, *J. Appl. Phys.* 102, 074115 (2007).
50. X. Lu, Q. Yang, C. Xiao, and A. Hirose, *Diamond Relat. Mater.* 16, 1623 (2007).
51. O. Auciello, *Nucl. Instrum. Met. Physics Res. B* 13, 561 (1986).
52. B. J. Waclawski, D. T. Pierce, N. Swanson, and R. J. Celotta, *J. Vac. Sci. Technol.* 21, 368 (1982).
53. S.-T. Lee, Z. Lin, and X. Jiang, *Mater. Sci. Eng.* 25, 123 (1999).
54. Sh. Michaelson, Y. Lifshitz, O. Ternyak, R. Akhvlediani, and A. Hoffman, *Diamond Relat. Mater.* 16, 845 (2007).
55. Sh. Michaelson, O. Ternyak, and A. Hoffman, *Appl. Phys. Lett.* 89, 131918 (2006).
56. J. Ristein, F. Maier, M. Riedel, M. Stammer, and L. Ley, *Diamond Relat. Mater.* 10, 416 (2001).
57. F. J. Himpsel, J. A. Knapp, J. A. Van Vechten, and D. E. Eastman, *Phys. Rev. B* 20, 624 (1979).
58. D. Takeuchi, H. Kato, G. S. Ri, T. Yamada, P. R. Vinod, D. Hwang, C. E. Nebel, H. Okushi, and S. Yamasaki, *Appl. Phys. Lett.* 86, 152103 (2005).
59. J. Chevallier, B. Theys, A. Lusson, C. Grattepain, A. Deneuville, and E. Gheeraert, *Phys. Rev. B* 58, 7966 (1998).
60. T. Lin, G. Y. Yu, A. T. S. Wee, and Z. X. Shen, *Appl. Phys. Lett.* 77, 2692 (2000).
61. J. R. Rabeau, P. John, and J. I. B. Wilson, *J. Appl. Phys.* 96, 6724 (2004).
62. J. Griffin and P. C. Ray, *Nanotechnology* 17, 1225 (2006).
63. P. W. May, J. N. Harvey, J. A. Smith, and Y. A. Mankelevich, *J. Appl. Phys.* 99, 104907 (2006).
64. P. W. May, M. N. R. Ashfold, and Y. A. Mankelevich, *J. Appl. Phys.* 101, 053115-1 (2007).
65. A. C. Ferari and J. Robertson, *Phys. Rev. B* 63, 121405 (2001).
66. S. M. Huang, Z. Sun, Y. F. Lu, and M. H. Hong, *Surf. Coat. Technol.* 151–152, 263 (2002).
67. Z. Sun, J. R. Shi, B. K. Tay, and S. P. Lau, *Diamond Relat. Mater.* 9, 1979 (2000).
68. M. S. You, F. C. N. Hong, Y. R. Jeng, and S. M. Huang, *Diamond Relat. Mater.* 18, 155 (2009).
69. E. J. Corat, R. C. Mendes de Barros, V. J. Trava-Airoldi, N. G. Ferreira, N. F. Leite, and K. Iha, *Brazil. J. Phys.* 27/A, 138 (1997).
70. S. Potocky, A. Kromba, J. Potmesil, Z. Remes, Z. Polackova, and M. Vanecek, *Phys. Status Solidi A* 203, 3011 (2006).
71. E. Kondoh, T. Ohta, T. Mitomo, and K. Ohtsuka, *Appl. Phys. Lett.* 59, 488 (1991).
72. B. V. Spitsyn, L. L. Bouilov, and B. V. Deryagin, *J. Cryst. Growth* 52, 219 (1981).
73. Y. Mitsuda, T. Yoshida, and K. Akashi, *Rev. Sci. Instrum.* 60, 249 (1989).
74. D. W. Kweon, J. Y. Lee, and D. Kim, *J. Appl. Phys.* 69, 8329 (1991).
75. K. A. Snail and C. M. Marks, *Appl. Phys. Lett.* 60, 3135 (1992).
76. A. Yamaguchi, M. Ihara, and H. Komiyama, *Appl. Phys. Lett.* 64, 1306 (1994).
77. Y. Muranaka, H. Yamashita, and H Miyadera, *Diamond Relat. Mater.* 3, 313 (1994).
78. C. J. Chu, R. H. Hauge, J. L. Margrave, and M. P. D′Evelyn, *Appl. Phys. Lett.* 61, 1393 (1992).
79. J. Petherbridge, P. May, S. R. J. Pearce, K. N. Rosser, and M. R. Ashfold, *J. Appl. Phys.* 89, 1484 (2001).
80. J. Lee, B. Y. Hong, R. Messier, and R. W. Collins, *J. Appl. Phys.* 80, 6489 (1996).
81. F. Behrendt, O. Deustchamn, B. Ruf, and J. Warnatz, *J. Vac. Sci. Technol. A* 14, 1604 (1996).
82. B. Ruf, F. Behrendt, O. Deutschmann, and J. Warnatz, *Surf. Sci.* 352–354, 602 (1996).
83. B. Ruf, F. Behrendt, O. Deustschmann, S. Kleditzsch, and J. Warnatz, *Proc. Combust. Inst.* 28, 1455 (2000).
84. C. J. Chu, R. H. Hauge, J. L. Margrave, and M. P. D. Evelyn, *Appl. Phys. Lett.* 61, 1393 (1992).
85. O. A. Williams, M. Daenen, J. D′Haen, K. Haenen, J. Maes, V. V. Moshchalkov, M. Nesládek, and D. M. Gruen, *Diamond Relat. Mater.* 15, 654 (2006).
86. A. C. Ferrari and J. Robertson, *Phys. Rev B* 63, 121405-1 (2001).
87. K. L. Ma, W. J. Zang, Y. S. Zou, Y. M. Chong, K. M. Leung, I. Bello, and S. T. Lee, *Diamond Relat. Mater.* 15, 626 (2006).
88. T. S. Yang, J. Y. Lai, C. L. Chen, and M. S. Wong, *Diamond Relat. Mater.* 10, 2161 (2001).
89. G. M. Mikheev, R. G. Zonov, A. N. Obraztsov, and D. G. Kalyuzhny, *Instrum. Exp. Tech.* 51, 456 (2008).
90. E. F. Antunes, A. O. Lobo, E. J. Corat, V. J. Trava-Airoldi, A. A. Martin, and C. Verissimo, *Carbon* 44, 2202 (2006).
91. L. V. Azaroff, "Elements of X-ray Crystallography," New York: McGraw-Hill, 1968.
92. K. L. Ma, W. J. Zang, Y. S. Zou, Y. M. Chong, K. M. Leung, I. Bello, and S. T. Lee, *Diamond Relat. Mater.* 15, 626 (2006).
93. T. S. Yang, J. Y. Lai, C. L. Chen, and M. S. Wong, *Diamond Relat. Mater.* 10, 2161 (2001).
94. S. Bühlmann, E. Blank, R. Haubner, and B. Lux, *Diamond Relat. Mater.* 8, 194 (1999).
95. R. Haubner and B. Lux, *Int. J. Refract. Met. Hard Mater.* 20, 93 (2002).
96. H. Windischmann, G. F. Epps, Y. Cong, and W. Collins, *J. Appl. Phys.* 69, 2231 (1991).
97. D. S. Dandy and M. E. Coltrin, *J. Appl. Phys.* 76, 3102 (1994).
98. M. You, F. C. Hong, Y. Jeng, and S. Huang, *Diamond Relat. Mater.* 18, 155 (2009).
99. V. Morlet, A. Kromba, R. Krates, J. Rosa, V. Vorlicek, J. Zemek, and M. Vanecek, *Diamond Relat. Mater.* 13, 604 (2004).
100. A. F. Azevedo, S. C. Ramos, M. R. Baldan, and N. G. Ferreira, *Diamond. Relat. Mater.* 17, 1137 (2008).
101. P. W. May and Y. A. Mankelevich, *J. Appl. Phys.* 100, 024301 (2006).
102. D. C. Barbosa, P. R. Barreto, P. Hammer, V. J. Trava-Airoldi, and E. J. Corat, *Diamond Relat. Mater.* [submitted].
103. R. J. Kee, F. M. Rupley, and J. A. Miller, "Chemkin-II: A fortran chemical kinetics package for the analysis of gas-phase chemical kinetics," Technical Report SAND89–8009, Sandia National Laboratories, 1990.
104. J. S. Kim, "Combustion Synthesis of Diamond," PhD thesis, Stanford University, Mechanical Engineering Department, 1998.
105. T. Kawato and K. Kondo, *Jpn. J. Appl. Phys.* 26, 1429 (1987).
106. S. J. Harris, *J. Appl. Phys.* 65, 3044 (1989).
107. D. C. Barbosa, H. F. Villa-Nova, and M. R. Baldan, *Brazil. J. Phys.* 36, 313 (2006).